UvA-DARE (Digital Academic Repository)

Scattering of hydrogen atoms from liquid-helium surfaces

Berkhout, J.J.; Walraven, J.T.M.

Link to publication

Scattering of hydrogen atoms from liquid-helium surfaces

J. J. Berkhout and J. T. M. Walraven

Universiteit van Amsterdam, Van der Waals–Zeeman Laboratorium, Valckenierstraat 65/67,
1018 XE Amsterdam, The Netherlands

We analyze in detail experiments in which we study the interaction of atomic hydrogen with liquid-helium surfaces. A theoretical background and a description of the experimental setup is given. A first experiment measured the transmission of hydrogen atoms through a capillary in the temperature interval of $145 < T < 526$ mK for ^{4}He surfaces and $73 < T < 174$ mK for ^{3}He surfaces. To extract the thermally averaged sticking probability s we need a model relating the atomic sticking coefficient $s(\mathbf{v})$ to the capillary transmission K. We analyze our data with a model based on a fixed $s(\mathbf{v})$, resulting in $s = 0.33(3)T$, and a model based on a speed-dependent $s(\mathbf{v})$, resulting in $s = 0.65(6)T$. The data show s to be linearly dependent on temperature. We do not observe any significant difference in s between ^{4}He and ^{3}He surfaces. In a second experiment we used a hemispherical liquid-helium covered quartz mirror to focus a hydrogen atom beam. The resolution of our setup is about 10 mrad, which is sufficient to study direct near-elastic scattering, providing precision data for the sticking coefficient is available.

I. INTRODUCTION

Scattering hydrogen atoms from the surface of liquid helium has attracted interest from a variety of physical fields.[1-5] The topic originates in studies of (spin-polarized) hydrogen at low temperatures, where inelastic scattering processes provide the mechanism to exchange heat between bulk H gas and helium covered walls of a sample cell. In particular at high gas densities or at low temperatures, where recombination to the (solid) molecular state H_2 is most effective, substantial temperature differences may develop between gas and surface. This issue arises in experiments aimed at achieving Bose-Einstein condensation in electron spin-down polarized hydrogen (H↓) by compression methods.[6-12] In experiments to accumulate electron spin-up polarized hydrogen (H↑) using pure field confinement in a magnetic trap, walls provide a cooling mechanism during filling.[13-17] There one has to strike a subtle balance between cooling efficiency and flux losses due to surface recombination or spin relaxation.[18-20] From a more general point of view the scattering of hydrogen atoms from the surface of liquid helium may be regarded as a model system to study the low energy limit of atom surface scattering. Apart from beam-type scattering experiments experimental information may be extracted from data for the sticking coefficient s, defined as the probability that a colliding atom will be scattered into a surface bound state, or from the accommodation coefficient α, characterizing the energy transfer per collision.

In this article we analyze two series of experiments in which we addressed the scattering of neutral hydrogen atoms from the surface of liquid helium in the temperature regime where quantum effects dominate the physics. First we studied the effect of sticking on the flow of H gas through a capillary.[21] This capillary flow (CF) experiment proved that the average momentum of the atoms parallel to the capillary axis is largely conserved in the flow, which was interpreted to imply the presence of substantial specular reflection on the capillary surface. The second series of experiments were done to obtain additional support for this interpretation and to look for the presence of direct (nonsticking) inelastic scattering using an atomic mirror.[22] As the results of the CF experiment showed that reflection of H atoms at a surface turns out to be high and the influence of substrate roughness is not too important, the feasibility of this mirror reflection (MR) experiment became clear. Generally, information about the atom-surface collisions is best obtained by angularly resolved measurements of single atom-surface scattering for the whole range of angles of incidence. In the MR experiment the effect of individual collisions of atoms incident along the surface normal were observed by using the reflection of atoms at a mirror surface to focus an atomic beam. An experimental advantage of this approach is the relatively easy detection due to the large integrated intensity. In these experiments for the first time focusing of an atomic beam by means of a solid mirror could be demonstrated.

This article is organized as follows. First we summarize the theoretical and experimental background. Then we discuss the principle of our experiments and describe the detailed experimental setups. Section V deals with the measurements and their interpretation. The conclusions are given in Sec. VI.

II. BACKGROUND

If a H atom collides with a liquid-helium surface, in general three types of scattering processes may occur, two of which are inelastic; the third channel is elastic (see Fig. 1).

(a) Elastic scattering

(b) Inelastic direct scattering
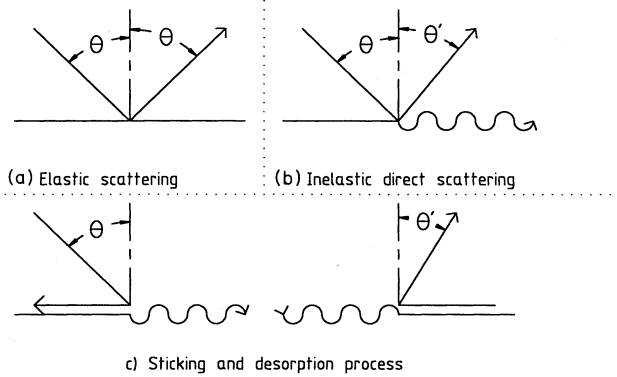
c) Sticking and desorption process

FIG. 1. Scattering of H atoms from a liquid-helium surface may be (a) elastic, (b) inelastic nonsticking, or (c) inelastic by sticking and desorption; θ is the angle of incidence of the atom, θ' the angle of reflection.

The elastic collisions, in which the energy and the momentum parallel to the surface are conserved, lead to specular reflection, be it that microscopic roughness may cause the reflection to appear as nonspecular with respect to the macroscopic substrate.

Inelastic scattering may be divided in direct inelastic processes in which the atom is reflected nonspecularly without adsorption, and sticking processes where the atom scatters into a surface bound state. In principle heat transfer is sensitive to both types of inelastic collisions. However, the direct inelastic channel is less efficient in this respect by a factor of order $(\epsilon_a/k_B T)^{-1.5}$ compared to the sticking channel (here ϵ_a is the surface adsorption energy and k_B is the Boltzmann factor).[23,24] For H on ^{4}He, $\epsilon_a = 1.00(2)$ K,[25] so the energy transfer of this process becomes quickly unimportant for temperatures below 500 mK. Also the momentum transfer parallel to the surface will become very small, so its influence on the capillary flow will be negligible. Nevertheless, as we shall argue in this paper the probability for near-elastic scattering may remain important at lower temperatures for experiments discriminating between elastic and near-elastic scattering. This view is supported by calculations.[26,27]

Experimentally the sticking process is characterized by the sticking coefficient s, defined as the probability that a colliding atom will enter a surface bound state. The heat transfer is characterized by the accommodation coefficient α which is defined as

$$\alpha = \lim_{T_g \to T_w} \frac{\dot{Q}_g - \dot{Q}_o}{\dot{Q}_g - \dot{Q}_w} , \tag{1}$$

where $\dot{Q}_g$ is the average kinetic energy flux (heat flux) carried by the incident gas atoms, T_g is the gas temperature, $\dot{Q}_o$ the outgoing heat flux, and $\dot{Q}_w$ the outgoing heat flux if all incident atoms are thermalized on the surface at temperature T_w. For $T_g \approx T_w$ the net heat flux from gas to surface is given by

$$P \approx \alpha \Phi 2 k_B (T_g - T_w) , \tag{2}$$

with Φ the total incident atomic flux.

For a thermal gas of hydrogen atoms s was first determined by Jochemsen et al.[28,29] Using magnetic resonance they found $s = 0.046$ at $T \approx 200$ mK for ^{4}He surfaces and $s = 0.016(5)$ for ^{3}He surfaces at $T \approx 100$ mK. Salonen et al. measured ballistic heat transport with a time-resolved method and found $\alpha = 0.2(1)$ for H on ^{4}He.[30] In a subsequent steady-state heat flux experiment Salonen et al. (SJKTT) obtained $\alpha = 0.19(5)$ for $T = 440$ mK.[31] Bell et al. found α to decrease from $\alpha = 0.8(4)$ at 600 mK to $\alpha = 0.4(2)$ at 275 mK.[9] Helffrich et al. also found a decreasing α for decreasing temperature in the range 180–400 mK with a SJKTT-type experiment.[32] Recently Doyle et al. extended the temperature range studied by 3 orders of magnitude. They observed an increasing sticking coefficient with decreasing temperature up to a value of $s = 0.30$ at $T = 100$ μK.[33] We noted slightly different definitions of α by the various authors.

The interpretation of the experiments mentioned in the previous paragraph is primarily based on a model in which H atoms either scatter elastically or enter a surface bound state (the sticking process) under emission of a single ripplon. The adsorption potential only supports a single bound state.[34,35] The adsorbed atoms are not localized in directions parallel to the surface but behave as the atoms of a nearly free two-dimensional gas.[36] The wave function of an adsorbed atom may therefore be written as

$$\Psi_\mathbf{k}(\mathbf{R}, Z) = A^{-1/2} \exp(i\mathbf{k} \cdot \mathbf{R})\phi(Z) , \tag{3}$$

in which $\mathbf{k}$ is the component of the wave vector parallel to the surface, $\mathbf{R}$ is the two-dimensional position vector, Z is the distance to the surface reference plane with area A, and $\phi(Z)$ is a function describing the Z dependence of the wave function. The sticking of the atoms leads to a surface density n_S which in thermal equilibrium is related to the volume density n_V by the surface adsorption isotherm. For volume densities of practical interest in our experiments this surface adsorption isotherm may be written as[37]

$$n_S = n_V \lambda_{\text{th}} \exp(\epsilon_a/k_B T) , \tag{4}$$

where $\lambda_{\text{th}} = (2\pi\hbar^2/mk_B T)^{1/2}$ is the thermal wavelength (m is the mass of the hydrogen atom). As was first pointed out by Kagan and Shlyapnikov, the adsorption process is accompanied by the excitation of a single ripplon and not significantly by the excitation of phonons.[38] The ratio of double ripplon emission to single ripplon emission for the adsorption process was estimated by Statt to be about 0.2.[39] The dispersion relation for the ripplons on a layer of helium covering a horizontal substrate is given by[40,41]

$$\omega_q^2 = \left[\left(g + \frac{3\alpha}{m_{\text{He}} d^4}\right) q + \frac{\gamma}{\rho_0} q^3\right] \tanh(qd) , \tag{5}$$

with ω_q the ripplon frequency, q the ripplon wave number, g the gravity acceleration, α the van der Waals attractive constant (which is of the order of

2×10^{-50} J m^3),[42] d the helium film thickness, $\gamma = 3.54 \times 10^{-4}$ J m^{-2} the ^{4}He surface tension at $T < 0.5$ K,[43,44] and $\rho_0 = 145$ kg m^{-3} the ^{4}He bulk density. Except for ^{4}He layers thicker than approximately 1 μm the van der Waals contribution dominates the gravity contribution in Eq. (5). For typical ^{4}He films of about 100 Å thickness the gravity contribution is 8 orders of magnitude smaller than the van der Waals contribution. The van der Waals attraction also dominates over capillarity for ripplon wavelengths of order 4000 Å and larger. The hyperbolic tangent incorporates the effect of the film thickness on the ripplon dispersion. Ripplons with wavelengths comparable to or smaller than this thickness behave as those on bulk liquid.

In the adsorption process a substantial part of the binding energy is converted into kinetic energy of the atom in the adsorbed state. This is illustrated in Fig. 2, in which the dispersion curves for ripplons and adsorbed atoms are plotted for the case of vanishing incoming kinetic energy ($E_k \ll \epsilon_a$). At the intersection of these curves both the momentum parallel to the surface and the energy are conserved, atom and ripplon having equal but opposite momentum. The intersection point corresponds to a ripplon with a wavelength $\lambda_r = 47$ Å and an atom with a kinetic energy $E^*/k_B = 423$ mK. Thus, for the sticking process on a typically 100 Å thick film the gravitational acceleration, the van der Waals term and the thin film factor tanh(qd) are not important, reducing Eq. (5) to

$$\omega_q^2 = (\gamma/\rho_0)q^3 . \tag{6}$$

After adsorption, two possible situations may occur. The atom may be evaporated by interaction with a ripplon while still in the energetic state E^* or thermalize through ripplon interaction before it is evaporated at a
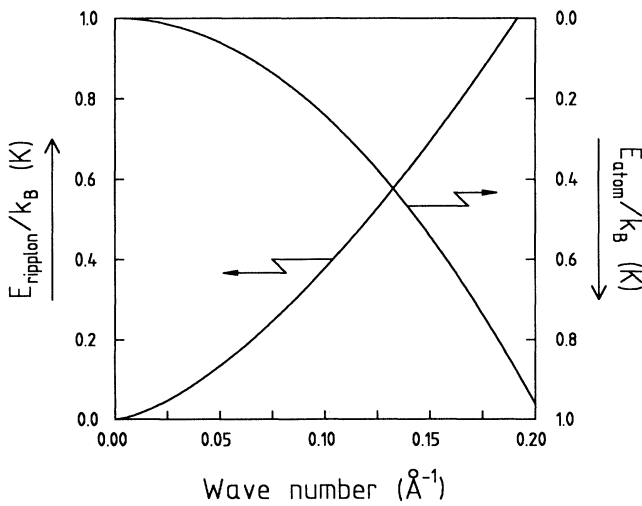

FIG. 2. Plot of the dispersion relations of ripplons on a ^{4}He surface (left axis) and H atoms (right axis). At the intersection the sum of the kinetic energies of the H atom and the ripplon equals the binding energy of the H atom on the helium surface.

later stage. Zimmerman and Berlinsky calculated the mean time between ripplon interactions for a H atom on the ^{4}He surface to range from 8.7×10^{-10} s at 400 mK to 2.4×10^{-8} s at 100 mK, much shorter than the mean residency time on the surface τ_a which ranges from 1×10^{-8} s at 400 mK to 3×10^{-4} s at 100 mK.[40] An expression for τ_a,

$$\tau_a = \frac{2\pi\hbar}{sk_BT} \exp(\epsilon_a/k_BT) , \tag{7}$$

is obtained by balancing the flux of sticking atoms $\Phi_s \equiv s\Phi$ against the flux of desorbing atoms $\Phi_d = n_S A \tau_a^{-1}$ for thermal equilibrium conditions. Here $\Phi = \frac{1}{4}n_V \bar{v}A$ is the total incident flux of atoms with A the surface area and $\bar{v} = (8k_BT/\pi m)^{1/2}$ is the average atomic speed.

The sticking probability was first calculated by Zimmerman and Berlinsky[36] and Kagan and Shlyapnikov.[38] Recent calculations by Hijmans, Walraven, and Shlyapnikov[45] and Carraro and Cole[46] discuss the sticking probability on helium films, taking into account the effects of the substrate. The more general problem of calculating the accommodation coefficient has been addressed by Kagan et al.,[23] Statt,[39] and Goldman.[47] In these theories the helium surface is treated as the surface of an incompressible liquid with a sharp density profile

$$\rho(\mathbf{r}, z) = \rho_0 \theta[z + h(\mathbf{r})] . \tag{8}$$

Here $\mathbf{r}$ is the two-dimensional position vector in the plane of the surface, z is the coordinate perpendicular to the surface, and $\theta(z)$ is the unit step function. Note that for a surface with a smooth density profile the use of the error function instead of the unit step function is more appropriate. The height fluctuations of the surface $h(\mathbf{r})$ may be expressed in terms of the elementary surface excitations, the ripplons, using a normal mode decomposition:

$$h(\mathbf{r}) = \frac{1}{\sqrt{A}} \sum_{\mathbf{q}} h_{\mathbf{q}} e^{i\mathbf{q}\cdot\mathbf{r}} , \tag{9}$$

with $\mathbf{q}$ the ripplon wave vector. The ripplon amplitude $h_{\mathbf{q}}$ is expressed in terms of the ripplon creation $r_{\mathbf{q}}^\dagger$ and annihilation $r_{\mathbf{q}}$ operators as

$$h_{\mathbf{q}} = \left[\frac{\hbar q \tanh(qd)}{2\rho_0 \omega_q} \right]^{1/2} (r_{\mathbf{q}}^\dagger + r_{-\mathbf{q}}) . \tag{10}$$

The effective surface-atom interaction for an atom at position $(\mathbf{R}, Z)$ with $\mathbf{R}$ the two-dimensional vector along the surface is given in linear approximation by

$$U(\mathbf{R}, Z) = U_0(Z) - \frac{1}{\sqrt{A}} \sum_{\mathbf{q}} h_{\mathbf{q}} \exp(i\mathbf{q}\cdot\mathbf{R}) \frac{\partial U_q(Z)}{\partial Z} , \tag{11}$$

with $U_0(Z)$ the static potential of a flat surface, and $U_q(Z)$ defined as

$$U_q(Z) = n_{\text{He}} \int e^{i\mathbf{q}\cdot\mathbf{r}} \int V(\{r^2 + [Z - z]^2\}^{1/2})\theta(z)dz\,d^2r , \tag{12}$$

where n_{He} is the helium atom density. The interaction Hamiltonian in second quantized form is given by

$$H_{int} = \frac{1}{\sqrt{A}} \sum_{\sigma',\sigma,\mathbf{q},\mathbf{k}} \hbar_{\mathbf{q}} \left\langle \sigma \left| \frac{\partial U_q(Z)}{\partial Z} \right| \sigma' \right\rangle a^{\dagger}_{\mathbf{k-q},\sigma'} a_{\mathbf{k},\sigma} ,$$

(13)

where σ is associated with the momentum of the H atom normal to the surface and may characterize the bound state or one of the continuum states. Far from the surface σ is the component of the wave vector normal to the surface and $E \cos^2 \theta = \hbar^2 \sigma^2 / 2m$. The adsorption rate $R(E, \theta)$ per atom may be calculated using first-order time-dependent perturbation theory:[36]

$$R(E, \theta) = \frac{2\pi}{\hbar A} \sum_{\mathbf{q}} \frac{\hbar q \tanh(qd)}{2\rho_0 \omega_q} \left| \left\langle B \left| \frac{\partial U_q(Z)}{\partial Z} \right| \sigma \right\rangle \right|^2$$

$$\times [(1 + n_{\mathbf{q}})(1 + N_{\mathbf{k-q}}) \delta(E + \epsilon_a - E_f - \hbar\omega_q) + n_{\mathbf{q}}(1 + N_{\mathbf{k+q}}) \delta(E + \epsilon_a - E_f + \hbar\omega_q)] ,$$

(14)

with $\langle Z|B \rangle$ the bound-state wave function of the atom with kinetic energy E_f and $\langle Z|\sigma \rangle$ the free-state wave function. Further, $n_{\mathbf{q}}$ is the occupation number for rip-plons with momentum $\hbar\mathbf{q}$ and $N_{\mathbf{k-q}}$ ($\ll 1$) is the analogous function for the H atoms. As the wavelength of the ripplons involved in the transition from the free to the bound state of the H atoms (47 Å) is smaller than the wavelength of thermal ripplons (typically 100 Å at 200 mK) the thermal occupation of these states is vanishing ($n_{\mathbf{q}} \ll 1$). For the adsorption process the surface therefore may be considered to be in its ground state over the temperature range covered by our experiments. The sticking probability is obtained by normalizing the transition rate to the incident flux:

$$s(E, \theta) = \frac{V R(E, \theta)}{A(E/2m)^{1/2} \cos\theta} ,$$

(15)

with V the volume of the sample cell. For low temperatures ($k_B T \ll \epsilon_a$) the matrix element is proportional to σ, so in this limit

$$s(E, \theta) = s_0 E^{1/2} \cos\theta$$

(16)

or

$$s(\mathbf{v}) = s_0 (\tfrac{1}{2} m v^2)^{1/2} \cos\theta ,$$

(17)

where s_0 is a proportionality constant. The thermally averaged sticking coefficient for incoming atoms at an angle θ with the normal on the surface, $s(T, \theta)$, and the overall thermally averaged sticking coefficient, $s(T)$, follow from integrating $s(\mathbf{v}) P_{in}(T, \mathbf{v}) d\mathbf{v}$, in which $P_{in}(T, \mathbf{v})$ is the normalized velocity distribution of the incoming atomic flux at temperature T. For a Maxwell-Boltzmann gas we find

$$P_{in}(T, \mathbf{v}) d\mathbf{v} = \left(\frac{m}{k_B T} \right)^2 \frac{v \cos\theta \exp(-mv^2/2k_B T)}{2\pi} d\mathbf{v} .$$

(18)

By calculating $s(T, \theta)$ and $s(T)$ we find for the angular dependence

$$s(T, \theta) = \tfrac{3}{2} s(T) \cos\theta .$$

(19)

As found by Zimmerman and Berlinsky the dependence of $s(E, \theta)/\cos\theta$ continues to be weakly dependent on θ even for higher temperatures, so Eq. (19) holds for higher temperatures as well.[36] Equation (16) also leads to the

thermal average of s, $s(T)$, being proportional to $T^{1/2}$ in the low-temperature limit. However, Goldman showed that s is strongly dependent on the long-range part of the interaction potential with the surface, and due to resonant enhancement of the sticking process the low-temperature limit for some potentials is only reached for $T \ll 1 \mu K$.[47] For helium films such resonances may be induced by the substrate potential as discussed by Hijmans et al.[45] and Carraro and Cole.[46]

In the regime where direct inelastic scattering is unimportant, that is for temperatures below 500 mK, Eq. (1) may be used to relate the accommodation coefficient to the sticking coefficient. From the Boltzmann distribution follows

$$\dot{Q}_g = 2k_B T_g \Phi$$

(20)

and

$$\dot{Q}_w = 2k_B T_w \Phi ,$$

(21)

where Φ is the total incoming flux of atoms. The average outgoing heat flux $\dot{Q}_o$ depends on the distribution of incoming atoms $P_{in}(T_g, \mathbf{v})$ and that of the desorbing atoms $P_{out}(T_w, \mathbf{v})$. To find the velocity distribution of the desorbing atoms, we apply the principle of detailed balance: the incoming atomic flux $\Phi_{in}(\mathbf{v}) d\mathbf{v}$ must, in equilibrium conditions, exactly equal the outgoing flux $\Phi_{out}(\mathbf{v}) d\mathbf{v}$. The incoming flux follows from Eq. (18):

$$\Phi_{in}(\mathbf{v}) d\mathbf{v} = \Phi P_{in}(T, \mathbf{v}) d\mathbf{v} .$$

(22)

The outgoing flux consists of two contributions:

$$\Phi_{out}(\mathbf{v}) d\mathbf{v} = \Phi_{in}(\mathbf{v})[1 - s(\mathbf{v})] d\mathbf{v}$$

$$+ P_{out}(T, \mathbf{v}) d\mathbf{v} \int s(\mathbf{v}) \Phi_{in}(\mathbf{v}) d\mathbf{v} ,$$

(23)

the first part being the flux due to the specularly scattered atoms and the second part being due to the desorbed surface atoms. As, by definition,

$$s(T) = \frac{\int s(\mathbf{v}) \Phi_{in}(\mathbf{v}) d\mathbf{v}}{\int \Phi_{in}(\mathbf{v}) d\mathbf{v}} ,$$

(24)

this balance leads to the relation

$$s(\mathbf{v}) \Phi_{in}(\mathbf{v}) d\mathbf{v} = s(T) \Phi P_{out}(T, \mathbf{v}) d\mathbf{v}$$

(25)

or

$$s(\mathbf{v})P_{\mathrm{in}}(T,\mathbf{v})d\mathbf{v} = s(T)P_{\mathrm{out}}(T,\mathbf{v})d\mathbf{v} \ . \tag{26}$$

Like the outgoing atom flux the average outgoing heat flux $\dot{Q}_o$ also consists of two parts:

$$\dot{Q}_o = \Phi \int \tfrac{1}{2}mv^2 P_{\mathrm{in}}(T_g,\mathbf{v})[1 - s(\mathbf{v})]d\mathbf{v}$$
$$+\Phi s(T_g) \int \tfrac{1}{2}mv^2 P_{\mathrm{out}}(T_w,\mathbf{v})d\mathbf{v} \ . \tag{27}$$

Substitution of Eqs. (20), (21), and (27) in Eq. (1) results in

$$\alpha = \lim_{T_g \to T_w} \frac{1}{2k_B(T_g - T_w)}$$
$$\times \left[\int \tfrac{1}{2}mv^2 P_{\mathrm{in}}(T_g,\mathbf{v})s(\mathbf{v})dv \right.$$
$$\left. -s(T_g) \int \tfrac{1}{2}mv^2 P_{\mathrm{out}}(T_w,\mathbf{v})dv \right] \ . \tag{28}$$

Using Eq. (26) this results in

$$\alpha = \frac{s(T_w)}{2k_B} \left. \frac{d}{dT} \right|_{T=T_w} \frac{1}{s(T)} \int \tfrac{1}{2}mv^2 s(\mathbf{v})P_{\mathrm{in}}(T,\mathbf{v})d\mathbf{v} \ . \tag{29}$$

To reduce this expression we find an expression for $\tfrac{1}{2}mv^2 P_{\mathrm{in}}(T,\mathbf{v})$ by differentiating Eq. (18) with respect to T:

$$\tfrac{1}{2}mv^2 P_{\mathrm{in}}(T,\mathbf{v}) = 2k_B T \left[P_{\mathrm{in}}(T,\mathbf{v}) + \tfrac{1}{2}T\frac{d}{dT}P_{\mathrm{in}}(T,\mathbf{v}) \right] \ . \tag{30}$$

By substituting this result in Eq. (29) and using Eq. (24) we find

$$\alpha = s(T_w) \left. \frac{d}{dT} \right|_{T=T_w} \frac{T}{s(T)} \left[s(T) + \frac{1}{2}T\frac{d}{dT}s(T) \right] \ , \tag{31}$$

or, after some straightforward differentiation

$$\alpha(T) = s(T) \left[1 + \frac{1}{2}\frac{d\ln s(T)}{d\ln T} + \frac{1}{2}\frac{d^2 \ln s(T)}{(d\ln T)^2} \right] \ . \tag{32}$$

This expression enables the comparison of all experimental results on the sticking coefficient with those on the accommodation coefficient. For the linear temperature dependence of s observed in our experiments this relation reduces to $\alpha(T) = \tfrac{3}{2}s(T)$. An equivalent form of this expression has been given by Goldman.[47]

The theory as described above may also be used to calculate the amount of direct inelastic scattering. The direct inelastic scattering rate may be found by replacing $\langle Z|B \rangle$ with $\langle Z|\sigma\prime \rangle$ in Eq. (14), taking $N(\mathbf{k})$ to be the density of bulk atom states, and adapting the sum over final states to bulk instead of bound states. For direct inelastic scattering over small angles the density of states of thermal ripplons is not negligible. Furthermore, the ripplons involved in this type of scattering have large wavelengths, so both the van der Waals term and the thin film factor

in Eq. (5) have to be taken into account and the use of the reduced equation (6) is not allowed anymore. A calculation by Hijmans and Shlyapnikov shows that for atoms perpendicularly incident on the surface the probability for direct inelastic scattering becomes greater than the probability for sticking for scattering angles less than about 0.2 rad at 500 mK down to 0.1 rad at 100 mK.[26]

III. EXPERIMENTAL SETUP

In the CF experiment the aim was to determine $s(T)$. We use two volumes connected by a capillary (see Fig. 3). At the start of a measurement, one of the volumes, the buffer volume, contains a quantity of H gas. The second volume, the pump volume, is kept empty of H atoms at all times (by recombining them to H_2 molecules). The atoms travel through the capillary from the buffer volume to the pump volume. As the mean free path of the atoms is much larger than the dimensions of the capillary, the atomic flux Φ is determined by the capillary impedance, which should depend on the sticking coefficient. We extract the sticking coefficient either from the time constant of the resulting density decrease in the buffer volume or the time constant of the decreasing flux through the capillary.

The aim of the MR experiment was to determine the fraction of atoms reflected specularly from a surface after a single collision per atom. Again a geometry with a buffer volume and a pump volume was used (see Fig. 4). Atoms are loaded into the buffer volume, from which they may escape to the pump volume through a small diaphragm. In this pump volume a concave mirror is situated which acts to reflect all specularly scattering atoms back through the diaphragm into the buffer volume. In the ideal case with unit probability of specular reflection, this results in the absence of a density decrease in the buffer volume. In the actual situation, the decay of the stagnant density allows us to extract information about the scattering process.

IV. EXPERIMENTAL APPARATUS

A. General cryogenic system

Our experiments are carried out in an Oxford Instruments 1000 (1000 μmol/s maximum circulation) dilution
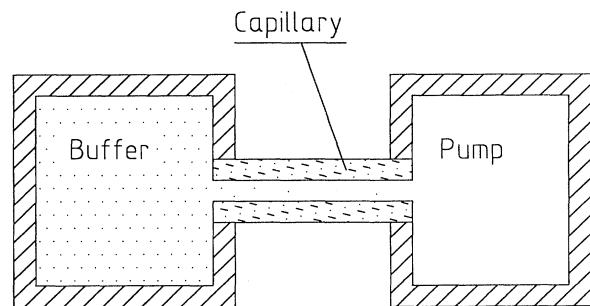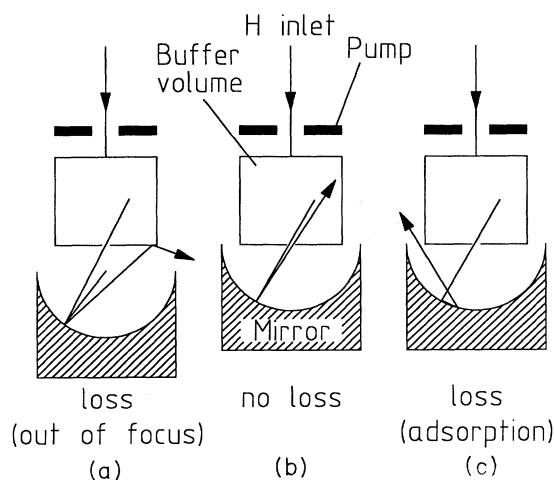

FIG. 3. The principle of the capillary flow experiment.

FIG. 4. The principle of the mirror reflection experiment.

refrigerator[48] with a maximum cooling power of 500 μW at a mixing chamber temperature of 100 mK and an unloaded base temperature of 4.5 mK (see Fig. 5). The sample cells were placed in the center of a 6 T superconducting magnet (Thor Cryogenics Ltd., 35 mm bore) with a homogeneity in the center of $1:10^4$ in a volume of at least 1 cm^3.

B. The capillary flow cell

A schematic drawing of the capillary flow cell used in the CF experiment is shown in Fig. 6. The cell body has been made of a low magnetic impurity-type copper and is connected to the mixing chamber by a 20 × 20 mm copper rod. The H atoms are produced by a room temperature discharge and fed into the cell from the bottom through a thin-walled German silver filling tube of 5.6 mm inner diameter. On their way to the cell the atoms pass two intermediate cooling stages, the accommodator, running at about 7 K, and the HEVAC, running at about 650 mK.[8] The H↓ atoms are driven to the high magnetic field region by field gradients and fluxing helium vapor and are collected in a buffer volume (V_b). Because of the difference in magnetic field between the dissociator (almost no field) and the cell (6 T) only high field seeking atoms enter the cell. Due to the relatively low concentration of magnetic impurities, some double polarization by preferential recombination of a states may occur. (The ground-state hyperfine levels are labeled a, b, c, and d in order of increasing energy.) However, any double polarization and subsequent change in relaxation rates is completely unimportant in this series of experiments in view of the relevant time scales involved.

All inner surfaces at cell temperature are covered with a liquid-helium film. An upper limit of 110 Å for the thickness of this film is calculated by assuming the helium content of the cell to be just short of being capable to form bulk liquid. This corresponds to the maximum allowed quantity of helium before its evaporation at higher temperatures in the fill tube gives rise to unacceptable heat loads on the cell.

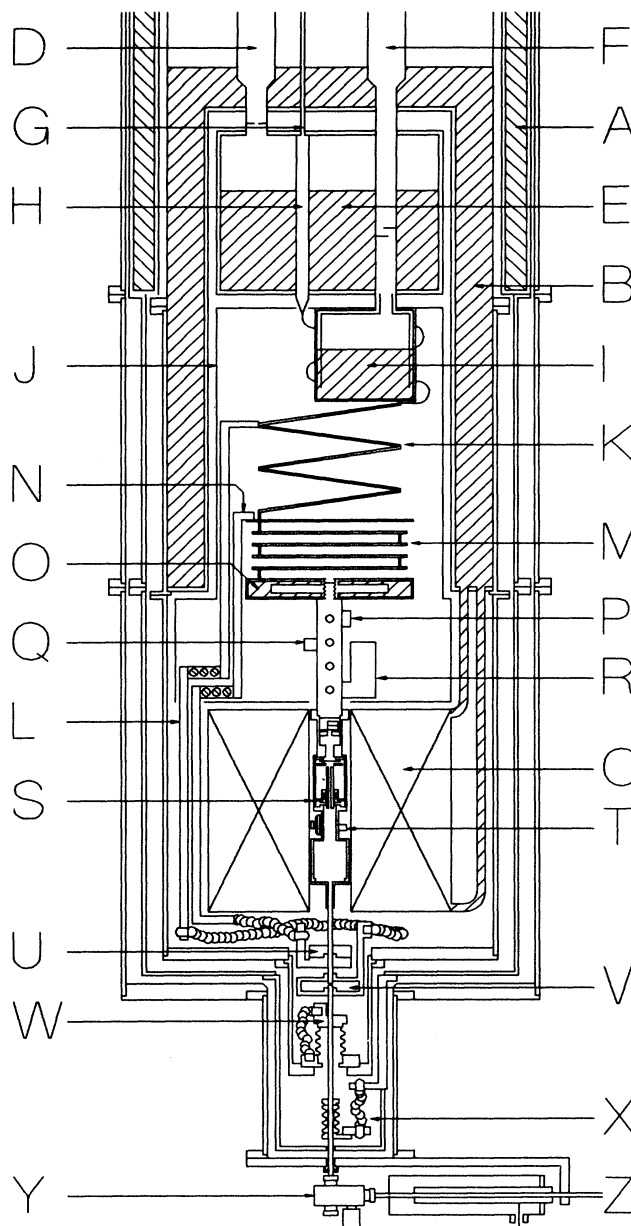The buffer volume contains a doped germanium bolometer[49] and a capacitive pressure transducer. The

FIG. 5. Schematic view of our dilution refrigerator cryostat. Explanation of symbols: A: Liquid-nitrogen bath (77 K); B: main He bath (4.2 K); C: main magnet; D: He pump line; E: pumped He bath (1.2 K); F: mixture pump line; G: mixture return line; H: condensor and condenser capillary; I: still; J: shield (800 mK); K: continuous heat exchanger; L: pinning (600 mK); M: discrete heat exchanger; N: pinning (200 mK); O: mixing chamber; P: cell heater; Q: upper cell thermometer; R: NBS fixed point device; S: CF cell; T: lower cell thermometer; U: thermal platform (about 300 mK); V: HEVAC (about 650 mK); W: accommodator (about 7 K); X: pinning (about 80 K); Y: Teflon valve; Z: room temperature dissociator.

pressure gauge, which was previously used by Van Yperen et al.,[50] has a sensitivity of 1.74 pF/Torr and a noise equivalent pressure of 5×10^{-7} Torr (one standard deviation at a bandwidth of 1.25 Hz) which corresponds to a minimum detectable density of 1×10^{13} cm^{-3} at 500 mK. The noise was due mainly to voltage noise originating in our General Radio capacity bridge. The pressure gauge also displayed long term drift, induced by changes in the magnetic field. The buffer volume was etched and thoroughly cleaned to free it from magnetic impurities, thereby reducing impurity relaxation (and subsequent recombination).[51] The effective volume of this compartment, defined as

$$V_b = \int_V [n(\mathbf{r})/n_0]d\mathbf{r}$$
$$= \int_V \exp\left(\frac{\mu_B[B(\mathbf{r}) - B_0]}{k_B T}\right) d\mathbf{r} , \qquad (33)$$

ranges from $V_b = 5.3(4)$ cm^3 at 70 mK to 10.0(1) cm^3 at 500 mK. Here B_0 and $B(\mathbf{r})$ are the magnetic fields at the entrance of the capillary and at position $\mathbf{r}$, respectively, n_0 and $n(\mathbf{r})$ are the corresponding atom densities, μ_B is

FIG. 6. The experimental cell for the capillary flow experiment.

the Bohr magneton, and T is the gas temperature.

Atoms will move from the buffer volume to the pump volume through the capillary, where they are subsequently removed by a pump plate (PP) which also serves as a flux detector. The PP detection method is described in detail elsewhere.[52] The flow capillary has a length of 21.97(3) mm, an inner diameter of 0.496(3) mm, and 1.1(1) mm outer diameter. Aiming for a smooth inner surface we used a commercial Pyrex capillary tube which was ground down to the specified outer diameter to fit inside the bore of a small superconducting magnet in the cell to throttle the capillary flow as described below. The main field is homogeneous to within 1:10^4 over the capillary region. The capillary is glued into a copper plate using Stycast 1266 epoxy.[53] To account for the difference in thermal contraction between the Pyrex and the copper, the thickness of the Stycast is chosen such that the combined thermal contraction of the Pyrex and the epoxy matches the thermal contraction of the copper closely over the whole temperature range from room temperature down to our operating temperature. A sufficiently accurate rule of thumb turns out to be $d = r/3$ (d the thickness of the epoxy between Pyrex and copper and r the radius of the capillary). Before gluing, the capillary was sealed off at one end, which enabled us to test the bond to the copper plate for leaks before cutting the capillary to its proper length and assembling the cell as a whole. The joint was found to be vacuum tight to temperatures below the lambda point, even after repeated cycling between room temperature and helium temperatures. It proved essential to roughen and clean the outer surface of the Pyrex thoroughly to obtain a good bond. For roughening the grinding procedure turned out to be sufficient, provided not too fine a grade was used. Cleaning was done ultrasonically using ethanol, acetone, and freon.

The flow through the capillary may be throttled by locally reducing the field to less than 5 T with a small magnet coil mounted around the capillary in the upper compartment. The coil has been wound with 12.500 turns of NIOMAX CN superconducting wire[54] with thickness of about 60 μm (including insulation) on a copper former with a bore of 1.2 mm. To reduce eddy currents, the former had a radial slit of 0.3 mm width, filled with Stycast 1266 epoxy. The turns were impregnated with Cyanolit 201. The Cyanolit cracks if cooled down, thereby enabling the liquid helium in the cell to cool the windings. The outer diameter of the coil was 11.8 mm. It is capable of producing a field of 1.3 T at a current of 1 A. By applying this field in the direction opposite to the main field, an energetic barrier for the H↓ atoms is created, thereby effectively isolating the lower part of the cell from the upper part. For a temperature of 200 mK we calculate a reduction of the atomic flux to about 9% due to the throttling field if we assume a sticking coefficient $s = 0$, and even to 3% if we assume $s = 1$. By observing the pressure decay with and without the throttling field we were able to verify that the intrinsic recombination in the cell was mostly due to recombination in the upper compartment. This pressure decay was completely dominated by the loss of atoms through the capillary when
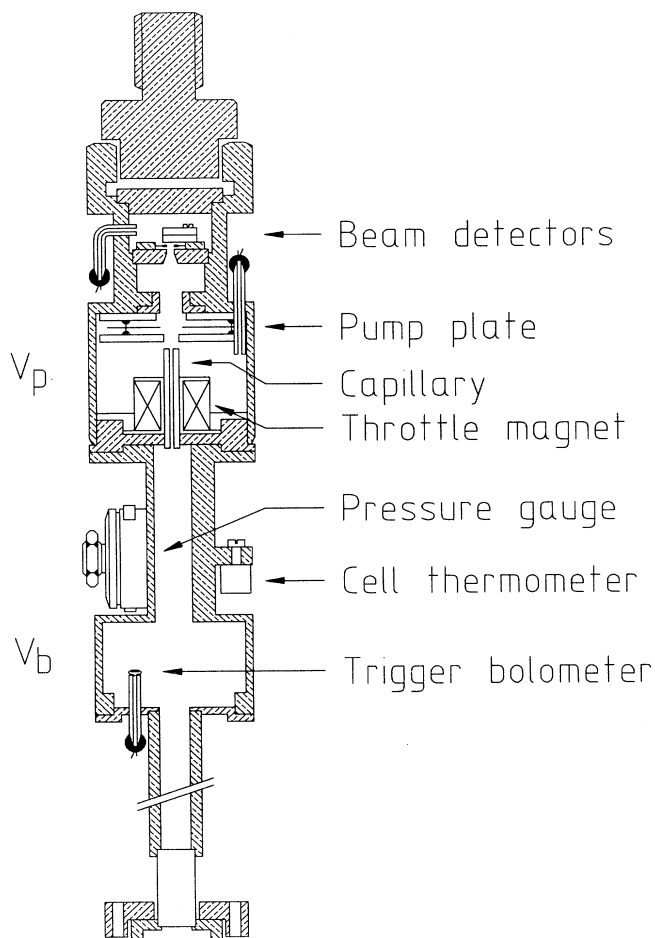
the PP detector was activated.

An assembly of two additional bolometers was also placed in the upper part. As these detectors were not used in the actual measurements, we omit further description in the current context.
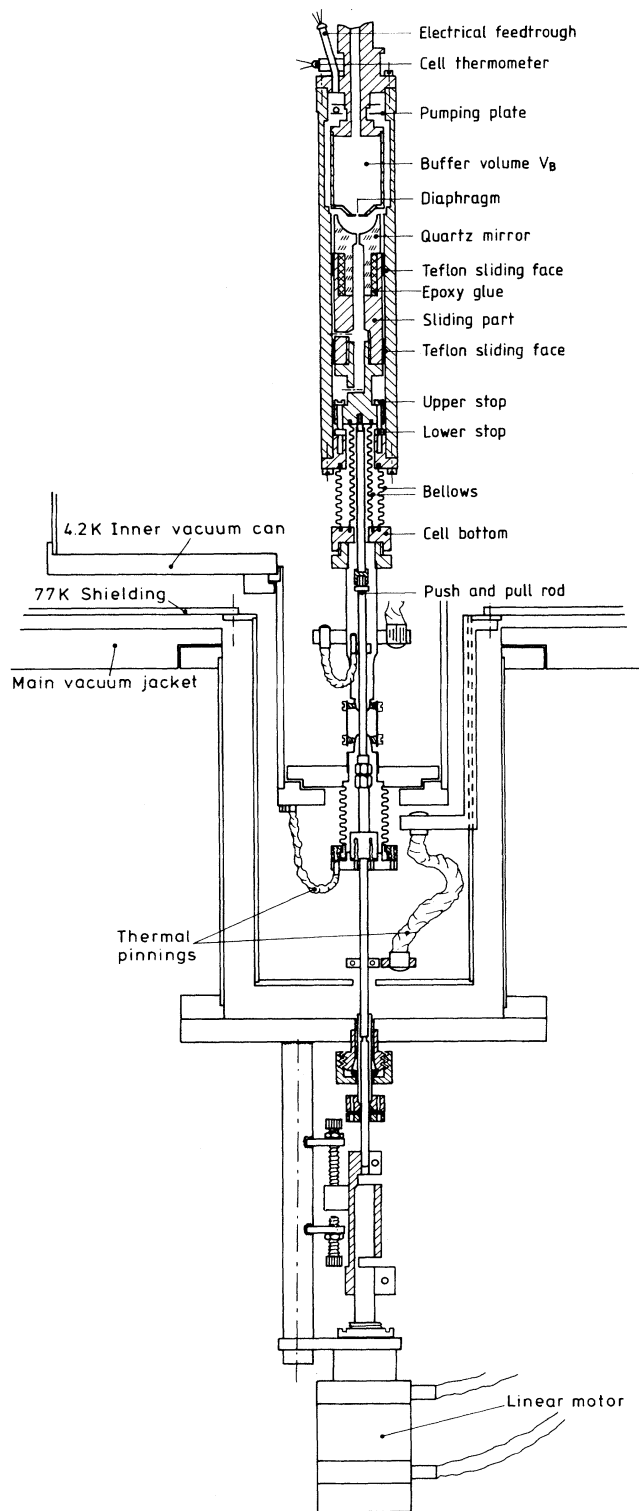

FIG. 7. The experimental cell for the mirror reflection experiment.

C. The mirror cell

The cell used in the MR experiment is shown in Fig. 7. In this case the buffer volume is separated from the pump volume by a diaphragm. The surfaces of the cell were again covered with a film by admitting into the cell a quantity of typically 0.02 cm^3 of liquid helium. This cell was connected to the mixing chamber by a 22 × 22 mm copper rod.

To produce the H atoms we changed over to a cryogenic RF dissociator operated at 600 mK and situated above the cell just outside the same 6 T superconducting magnet as used in the CF experiment. The dissociator was used in an earlier experiment by our group[14] except for the helix, which was replaced by a helix of thicker copper wire in order to improve cooling. This four-turn helix was 13.5(5) mm in height with an outer diameter of 9.1(1) mm and a pitch of 0.33 mm^{-1} and was made from 1.55(5) mm diameter uninsulated commercial copper wire. It was glued with Eccoshield VSM silver filled epoxy[53] into a pothole drilled in the dissociator flange. To couple the RF power into the helix, a one-turn coupling loop from a copper wire 0.75(5) mm diameter and an outer diameter of 8.6(1) mm was glued to the end of the inner conductor of the RF feed line with Eccoshield VSM. The loop and helix were wound in opposite sense for optimal coupling.[55] This resulted in a dissociator with resonance frequency of 773.2 MHz and a Q factor of 460 at room temperature. At 4.2 K the resonance had shifted to 776.5 MHz and the Q factor rose to 725. The H↓ flux entering the cell reached 1×10^{14} atm/s with an input peak power of 32 mW during a pulse of 120 μs and a repetition rate of 150 Hz. As the dissociation energy of H$_2$ is 4.5 eV, this corresponds to a dissociator efficiency of 6%. Crucial to starting the discharge proved a magnetic field exceeding 34 mT.

The dissociator is connected by a thin-walled stainless-steel tube of 6 mm diameter and 11 mm length to an intermediate cooling stage at about 200–400 mK, depending on the cell temperature. To effectively cool the atoms and to recondense the helium vapor coming from the dissociator, this cooling stage is configured as a labyrinth with four right turns in the path of the atoms. Just before this labyrinth a germanium trigger bolometer is located in order to enable quick removal of any atoms remaining in the dissociator region after filling the buffer volume.

The high field seeking atoms (a and b states) are forced into the buffer volume by the magnetic gradient of the main coil. In order to minimize recombination losses great care was exercised to avoid magnetic surface impurities in the buffer volume by using a low magnetic impurity-type copper[56] and careful etching and cleaning. Soldered to the bottom of the buffer compartment is a 50 μm thick copper foil containing a 0.25 mm radius orifice through which the atoms can escape to the pump volume. The effective buffer volume V_b [according to Eq. (33) with $B(0)$ at the diaphragm] ranges from 10.12 cm^3 at 80 mK to 10.39 cm^3 at 400 mK and is thus only very weakly dependent on temperature.

The pump volume contains a concave hemispherical fused quartz mirror with a radius of 9 mm, ground to

optical precision. If this mirror is perfectly aligned with the orifice, an angle of reflection of an atom of about 1° with respect to the normal is sufficient to let the reflecting atom miss the orifice. The mirror is mounted in a copper sliding piece using Stycast 1266. To account for thermal contraction, the thickness of the Stycast layer has been matched to the thickness of the mirror stem with the method described above. While the epoxy was cured, the position of the focus was aligned to the vertical axis of the sliding piece by a laser system to an accuracy of better than 50 μm. The sliding piece fits into the cell with a tolerance of less than 5 μm and can be moved up and down over a distance of about 4.8 mm.

At first the sliding surfaces were made of polished copper, but as this resulted in severe damage after moving the piece up and down several times before the start of the experiment, we changed the sliding surface to Teflon rings of about 0.5 mm thickness, fitting tightly on the copper substrate and fixed in position by a rim of Stycast 1266. To ensure smooth operation at low temperatures, it proved essential to polish the Teflon surface to a high finish. The sliding piece was connected to a push and pull mechanism extending to an inchworm motor situated at room temperature. This inchworm motor may be positioned with an accuracy of 0.5 μm relative to the cryostat outer shield. To prevent damage to mirror and diaphragm, the displacement of the sliding piece was limited by stops also functioning as internal reference points for the mirror position. To prevent the occurrence of a pool of liquid helium at the bottom of the mirror a 1.1 mm hole was drilled at the axis of the mirror. This channel is also used to insure efficient evacuation of the lower part of the cell.

The atoms not reflected back into the buffer volume will travel randomly in the pump volume and may reach a PP detector through a slit between the outer wall of the buffer compartment and the inner cell wall. This annular slit is 0.5 mm wide over a length of 1.2 mm, followed by a 2.5 mm wide section over 35 mm. The probability for an atom moving randomly in the pump volume to reenter the buffer volume is calculated to be at most 2% of that to reach the pump plate.

The pump plate used in the MR experiment is mounted around the neck of the buffer volume. The design deviates slightly from that described in Ref. 52. The plate is cut out of 50 μm thick copper foil and is suspended by three 16 μm tungsten wires. To try to reduce microphonic noise these wires were put under tension with stainless-steel springs exerting a force of 100–200 N at room temperature. This design turned out to be fairly shockproof. The operating temperature of the pump plate was 1.1 K with a heating power of typically 16 μW.

D. Surface roughness

Crucial to both experiments is the quality of the scattering surface, the inner surface of the capillary in the CF experiment, and the mirror surface in the MR experiment. In order to estimate this quality we used a scanning electron microscope with a maximum resolution of about 100 Å.

To determine the smoothness of the inner surface of the capillary used in the CF experiment, we put a sample of the same rod from which this capillary was made under the microscope. The results show a very smooth inner surface with no noticeable roughnesses of more than 100 Å in height except for some isolated grains of dirt and some scratches. For the test sample the total area of damaged or dirty surface was less than 1% of the total surface area. The nature of the scratches leads us to believe that they were the result of the mechanical abrasion necessary to prepare the test sample. Therefore, to our estimate, less than 0.1% of the inner surface of the capillary used in the cell was not smooth.

The mirror surface was itself checked for microscopic roughness. This required the evaporation of a layer of chromium (about 50 Å) followed by a layer of gold (about 200 Å) on the surface. The surface was found to be very smooth, except for some pores with typical dimensions 1 μm not exceeding 0.3% of the total area. These holes possibly are an intrinsic property of the type of fused quartz from which the mirror was made. We estimate that not more than 1% of the atoms are lost from the specular beam due to static surface irregularities, which is negligible to the loss due to other geometrical factors such as the coma of the mirror. As the metallic layer on the quartz was damaged chemically by H_2 gas in a preliminary stage of the experiment, we repeated the final polishing stages on the surface, using the bare quartz surface in the experiment.

We assume any irregularities of size less than 100 Å to be smoothed out by the helium film. To support this assumption, we numerically analyzed the behavior of a helium film over a solitary cylindrical obstacle with a radius of 100 Å and a height of 100 Å on top of an otherwise perfectly smooth surface. We assume the substrate potential to result from addition of pair interaction of a test particle with the individual substrate atoms. In our model we treated the substrate as a homogeneous mass distribution. If the contribution to the total van der Waals potential due to a volume element d^3x in the substrate is given by

$$dU_{\text{vdW}} = -\frac{6\alpha}{\pi r^6} d^3x \ , \tag{34}$$

integration over a half-infinite three-dimensional substrate results in the usual expression for the van der Waals potential $U_{\text{vdW}} = -\alpha/d^3$. We numerically integrated Eq. (34) to obtain the van der Waals potential $U_{\text{vdW}}(\mathbf{r}, z)$ for any position above our model substrate. The hydrostatic pressure p in an incompressible liquid covering this substrate is given by

$$p_{\text{vdW}}(\mathbf{r}, z) = -\rho_0[U_{\text{vdW}}(\mathbf{r}, z) - U_{\text{vdW}}(\text{ref})] \ , \tag{35}$$

where $U_{\text{vdW}}(\text{ref})$ is the van der Waals potential at the surface of the liquid at infinity (above the flat plane reference). The surface tension also contributes to the hydrostatic pressure. At the liquid-vapor interface this pressure is given by

$$p_\gamma = \gamma \left(\frac{1}{R_1} + \frac{1}{R_2} \right) , \qquad (36)$$

where R_1 and R_2 are the principal radii of curvature of the interface. As the gas and vapor pressures are negligible the total hydrostatic pressure at the surface has to be zero. The shape of the surface is therefore obtained from

$$p_{vdW}(\mathbf{r}, z) + p_\gamma(\mathbf{r}, z) = 0 , \qquad (37)$$

resulting in

$$\rho_0 [U_{vdW}(\mathbf{r}, z) - U_{vdW}(\text{ref})] = \gamma \left(\frac{1}{R_1} + \frac{1}{R_2} \right) . \qquad (38)$$

We calculated this shape numerically by relaxing the surface to zero total hydrostatic pressure for several film thicknesses. Figure 8(a) shows an example of a plot of the surface height as a function of distance to the center of the cylindrical obstacle for a film thickness of 60 Å. The angle of the film surface with respect to the plane of the substrate for this surface is shown in Fig. 8(b). The results for the maximum angle of the film surface with respect to the plane of the surface are given in Fig. 9 for several film thicknesses. For film thicknesses greater than
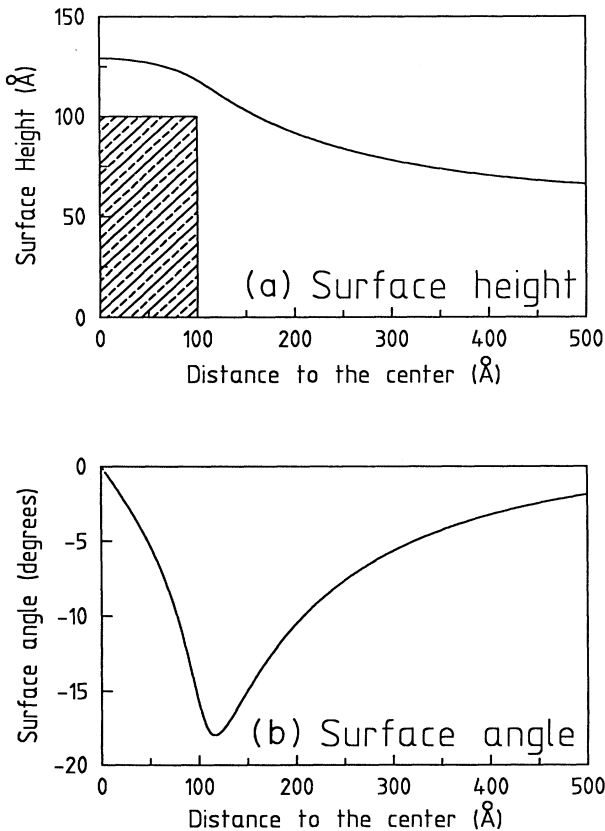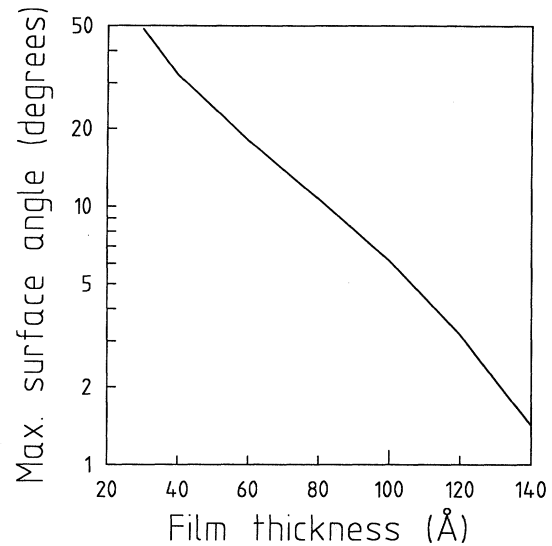

FIG. 9. Maximum angle with respect to the plane of the substrate of the film surface above a cylindrical obstacle as a function of film thickness.

about 120 Å this maximum angle, which is only reached in a small area, is smaller than 3°. A deviation of 3° for a specularly reflecting atom means that only after some tens of collisions an appreciable amount of momentum transfer parallel to the surface is achieved. We conclude that this amount of surface roughness is unimportant in the CF experiment for the temperature regime studied. As the resolution of the MR experiment is about 0.6°, this type of deviation might be of importance in this experiment. However, we believe that the total area thus affected is small enough to reduce the effect to a completely unimportant level. This assumption is supported by the observed reflectivity of the mirror as described below.

E. Thermometry

The temperature of each cell was monitored by two separate carbon resistors (Matsushita 200 Ω). One of these thermometers was situated on the copper connection rod between the cell and mixing chamber, in a region were the stray field of the 6 T coil was reduced to less than 0.1 T. The other thermometer was placed on the buffer compartment of the cell. The zero-field values of these thermometers were calibrated in previous runs against ^{3}He vapor pressure and a NBS SRM 768 fixed point superconducting device providing five separate reference temperatures consisting of the transition temperatures between the normal and superconducting states of samples of AuIn$_2$ (with transition temperature of 205.4 mK), AuAl$_2$ (162.53 mK), Ir (98.7 mK), Be (23.6 mK), and W (15.3 mK). Only the upper three reference points were actually used.

The Matsushita thermometer values were checked again in the CF experiment against the NBS device and in the MR experiment against a ^{3}He melting line ther-

FIG. 8. (a) Surface height of a ^{4}He film of 60 Å above a cylindrical obstacle of 100 Å as a function of the distance to the center of the obstacle; (b) angle of this film surface with respect to the plane of the surface.

mometer and turned out to be correct within 3 mK over the whole temperature range of interest. While calibrating these thermometers, we discovered an error in our previous assumptions regarding the NBS device. The transition temperature of the superconducting materials is specified for zero magnetic field and shift to lower temperatures with increasing field. The magnetic field also causes hysteresis, that is, the temperature of the transition going from lower to higher temperature is higher than the temperature of the transition while going from higher to lower temperature. This difference in temperature has a known linear relation to the magnetic field for low fields, and as the shift in critical temperature has a known linear relation to the field too, the true critical temperature may be obtained by determining the magnetic field from the hysteresis and correcting the critical temperature for this field. However, for sufficiently high magnetic fields, the hysteresis saturates, but the critical temperature keeps shifting. This leads to an underestimation of the actual magnetic field and thus to an underestimation of the shift in critical temperature. For the $AuIn_2$ transition, which shows the largest hysteresis of all five transitions, this saturation was found to occur at a field of the order of 23 μT. In our cryostat it turned out not to be possible to cancel the field sufficiently to enter the linear regime. We estimate that due to this effect our thermometry has an additional uncertainty of about 1 mK, which is small compared to the other sources of error. The field dependence of the thermometer calibrations was determined by comparing the thermometer in near-zero field to the thermometer in high field.

To facilitate the use of our melting line thermometer, we put additional temperature pinning points in the filling capillary. From the melting line thermometer itself at cell temperature, the capillary was pinned first to a point connected to the cold plate of the dilution refrigerator, then to a point having the temperature of the cell, and then to the cold plate pinning again. By including this last pinning point, it is not necessary anymore to let the cell temperature cross the temperature of the cold plate pinning point at exactly the temperature of the minimum in the melting line in order to avoid motion of the solid plug in the capillary. Instead, as long as the cold plate pinning point is kept lower in temperature than the cell until the latter passes the melting line minimum temperature, a strong solid plug in some part of the capillary (though not always the same part) is assured at any time.

V. MEASUREMENTS

A. Capillary flow experiments

In the CF experiments we determined the sticking probability as a function of temperature by measuring the capillary flow impedance by observing either the density decay (with the pressure gauge) or the hydrogen atom flux (with the PP detector).

Measuring with the pressure gauge the whole cell is first filled with H↓ up to a density $n \approx 2 \times 10^{15}$ cm^{-3}. Then the pump plate is heated to its operational temper-

ature and one monitors, after a short (< 1 s) transient due to the recombination of the gas in the pump volume, the exhaust of the buffer volume through the capillary. Since the area of the pump plate is much larger than the area of the entrance orifice of the capillary, the probability of the H↓ atoms to return to the buffer volume is negligibly small ($\ll 10^{-3}$). A typical pressure decay measurement is shown in Fig. 10.

Measuring with the pump plate one monitors the H flux during filling and decay. The sensitivity of this method is at least 3 orders of magnitude better than that of the pressure measurements. A typical pump plate measurement is shown in Fig. 11.

Neglecting recombination and gas collisions the flux Φ of atoms escaping V_b through the capillary is given by

$$\Phi = \tfrac{1}{4}n\bar{v}AK ,\tag{39}$$

with n the density in the buffer volume, $A = \pi a^2$ the area of the entrance orifice of the capillary of radius a, and K the transmission coefficient. This flux equals the rate of change of the number of atoms N in the buffer volume, leading to the density decay

$$dn/dt = -\tfrac{1}{4}Kn\bar{v}A/V_b = -n/\tau_1 ,\tag{40}$$

with τ_1 the time constant of the density decay. From our measurements we determined the time constants of the decay by a computer analysis. To correct for recombination in the buffer volume and collisions in the gas phase, we included a second-order decay term in the equation to be fitted:

$$dn/dt = -c_1 n - c_2 n^2 ,\tag{41}$$

with $c_1 \equiv \tau_1^{-1}$ and c_2 the first- and second-order decay constants. As c_1 is dominant, the flux depends linearly on the density and an equation of the form of Eq. (41) may be written for the flux decay as well. Equation (41) is integrated analytically and the result is fitted to the pressure or flux decay data to extract c_1 and c_2. Data were only collected in a temperature regime where the helium vapor pressure did not significantly impede the flow and recombination losses could be neglected.

We note that the fraction of the atoms entering the tube over the surface is small, 4.7% for ^{4}He surfaces at $T = 145$ mK. At this temperature the residency time τ_a is about 7 μs, which is much longer than the momentum
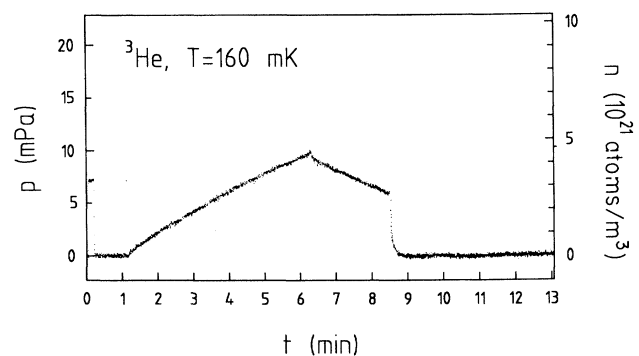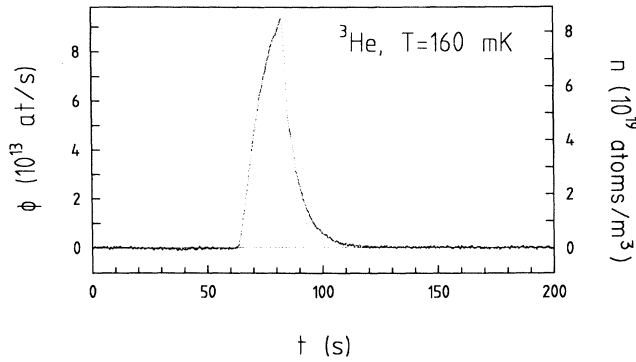

FIG. 10.   A typical pressure decay measurement.

FIG. 11. A typical flux decay measurement.

relaxation time 1.1 ns of the adsorbed atoms.[40] Hence the motion of the adsorbed atoms is diffusive and the mean square displacement from the adsorption site is negligibly small (about 5 μm).

Throughout this paper we neglect the effects associated with the finite transmission time through the capillary. This transmission time may be estimated by

$$\tau_{\rm tr} = \frac{2N_c a}{\bar{v}} , \tag{42}$$

where N_c is the average number of wall collisions a transmitted particle has undergone. For purely diffusive flow $N_c = L^2/(8a^2)$,[57] where L is the length of the capillary, we find $\tau_{\rm tr}$ ranges from 12 ms at 77 mK to 5 ms at 500 mK, much less than the observed density decay time constants. In the specular limit $N_c = L/a$ and $\tau_{\rm tr}$ is even smaller.

The role of wall collisions only enters into Eq. (40) through the transmission coefficient K. Assuming the atoms to scatter purely diffusively according to a cosine distribution (which corresponds to a sticking probability of one), one obtains the transmission coefficient calculated by Clausing (K_C). An accurate fitting formula for K_C is given by Berman:[58] defining $F \equiv L/a$, $G \equiv (F^2 + 4)^{1/2}$, and $H \equiv \ln([F + G]/2)$, then

$$K_C = 1 + \tfrac{1}{4}F(F - G) - \frac{[(8 - F^2)G + F^3 - 16]^2}{72FG - 288H} . \tag{43}$$

This coefficient K_C is purely determined by geometrical factors and thus temperature independent. In the Knudsen regime for long capillaries the Clausing factor is given by[59]

$$K_C \approx K_K = \frac{8a}{3L} . \tag{44}$$

The decay time constant τ_1 for $K = K_K$ would be

$$\tau_1 = \tau_{\rm max} = \frac{3LV_b}{2Aa\bar{v}} . \tag{45}$$

In the absence of momentum transfer parallel to the surface, as in the case of specular reflection, the transmission coefficient of the capillary becomes 1 and the decay time

constant τ_1 becomes

$$\tau_1 = \tau_0 \equiv \frac{4V_b}{A\bar{v}} . \tag{46}$$

For our capillary $L/a = 88.6(6)$ and therefore $K_C = 0.0284$, resulting in a maximum possible enhancement of the decay time by a factor of 35. The transmission coefficient K in the experiment follows as $K = \tau_0/\tau_1$. The observed decay times τ_1 typically are 5–10 s. The experimental results for K are given in Table I.

As the aim of this experiment is the determination of the sticking coefficient s we need to know the relation between K and s. In the case of $s = 0$, K remains 1 even for infinite capillary lengths, but for $s = 1$ the transmission coefficient K becomes the Clausing factor K_C and approaches the asymptote K_K. The relation $K(s)$ is given by De Marcus as approximately[60]

$$K(s) = K_C \frac{(K_C - 1)s + 2}{(1 - K_C)s + 2K_C} . \tag{47}$$

Inversion of this relation results in

TABLE I. The experimental results of the CF experiment for K vs T obtained with the pressure gauge and the PP detection method for all different helium contents of the cell.

Method	Cell contents	T (mK)	K
Pressure gauge	Pure ^{4}He	193(3)	0.391(32)
		213(3)	0.360(17)
		233(3)	0.338(14)
		263(3)	0.340(13)
		303(3)	0.309(17)
		353(3)	0.264(9)
		403(3)	0.258(11)
		453(3)	0.240(8)
		503(3)	0.236(6)
		528(3)	0.200(15)
Pressure gauge	0.2% ^{3}He	163(3)	0.459(29)
		182(3)	0.420(22)
		203(3)	0.391(22)
Pressure gauge	5% ^{3}He	164(3)	0.422(26)
PP method	Pure ^{4}He	146(3)	0.463(23)
		155(3)	0.429(19)
		164(3)	0.407(18)
		183(3)	0.387(17)
		213(3)	0.353(13)
		253(3)	0.334(11)
		323(3)	0.290(8)
PP method	5% ^{3}He	77(7)	0.551(55)
		92(6)	0.518(41)
		101(5)	0.495(34)
		110(5)	0.472(30)
		119(4)	0.466(27)
		128(4)	0.453(24)
		137(3)	0.437(22)
		146(3)	0.421(20)
		155(3)	0.422(20)
		164(3)	0.379(18)
		173(3)	0.374(17)

$$s(K) = \frac{2K_C(1-K)}{(K+K_C)(1-K_C)} \; . \tag{48}$$

Unfortunately, the use of this inverted formula may result in large relative errors in s for K close to 1. We therefore simulated the flow through the capillary by a one-speed test particle Monte Carlo computer simulation[61,62] in which we assumed the atom to have a probability s to stick to the surface and to scatter specularly otherwise. This assumption is justified in Sec. II. We calculated K as function of L/a for several values of s (see Fig. 12). We show in Fig. 13 the results of K versus s according to De Marcus and our simulation, calculated to within 1% using 10^5 particles. Our results are described within 3% by the empirical form

$$s = \frac{1-K}{1-K_C} \left[\frac{K_C}{K} \right]^{1/2} e^{(-3.915\Delta K)}(1+4.2\Delta K^2) \; , \tag{49}$$

where $\Delta K = K - K_C$.

The capillary flow simulation was based on the assumption that after sticking the atom is desorbed from the surface in a random direction according to a cosine distribution:

$$P(\theta,\phi)d\theta \, d\phi = 2\cos\theta(d\Omega/2\pi) \; . \tag{50}$$

In general, we should apply detailed balance to relate the velocity distribution of desorbing atoms $P_{out}(T,\mathbf{v})$ to the atomic sticking probability as in Eq. (26). For $s(\mathbf{v}) \equiv s(T)$ this equation leads to $P_{in}(T,\mathbf{v}) \equiv P_{out}(T,\mathbf{v})$, i.e., the particles will desorb from the surface according to a cosine distribution. This assumption [Eq. (50)] leaves no room for a temperature dependence of $s(T)$.

The results of the capillary flow experiment as published in an earlier report, based on the simulation assuming $s(\mathbf{v}) \equiv s(T)$ (the one-speed model), are summarized by the relation $s/T = 0.33(3)$ K^{-1} for 145 mK$<$ T $<$526 mK.[21] In view of the fact that the observed sticking coefficient is not temperature independent, the assumption of a fixed atomic sticking probability for each atom independent of its velocity and angle of incidence became suspect. The linear dependence of $s(T)$
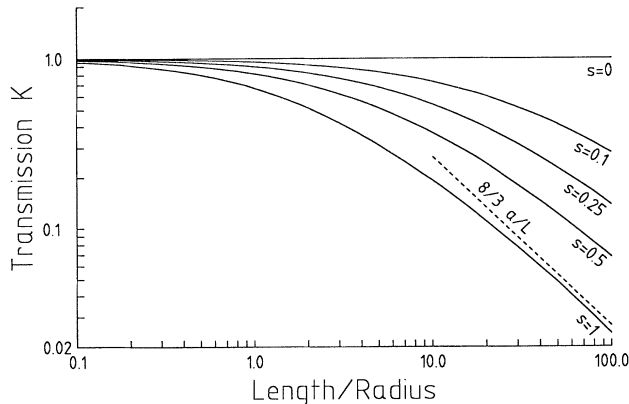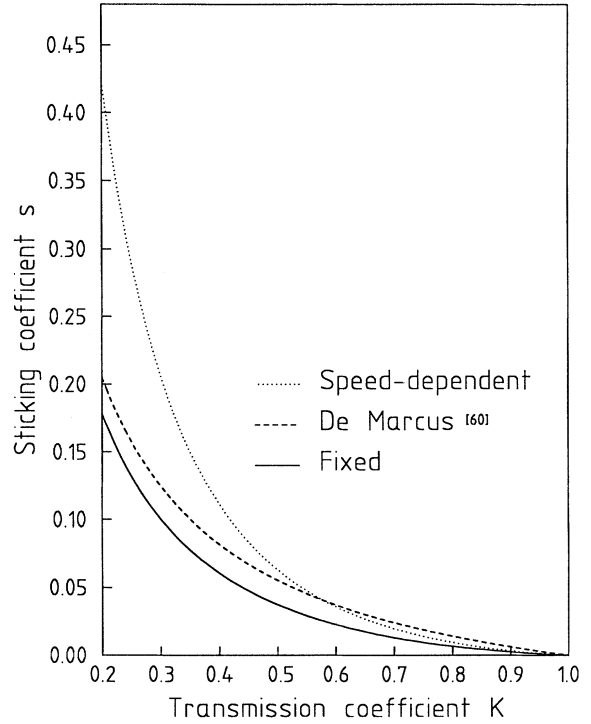

FIG. 13. The thermally averaged sticking coefficient s as a function of the transmission coefficient K according to (a) the De Marcus calculations (dashed line); (b) our model with fixed atomic sticking coefficients (solid line); (c) our model with velocity-dependent atomic sticking coefficients (dotted line).

on T suggests an atomic sticking probability of the form $s(\mathbf{v}) \sim v^2 \cos\theta$, with Eq. (24) resulting in

$$s(\mathbf{v}) = s(T)\left(\frac{3m}{8k_BT}\right) v^2 \cos\theta \; . \tag{51}$$

The distribution of desorbing atoms after sticking then should be

$$P_{out}(T,\mathbf{v})d\mathbf{v} = \frac{3}{2\pi}\left(\frac{m}{2k_BT}\right)^3$$
$$\times v^3 \cos^2\theta \exp\left(\frac{-mv^2}{2k_BT}\right) d\mathbf{v} \; . \tag{52}$$

We resimulated the capillary flow based on this model (the velocity-dependent model). The above formula for $s(\mathbf{v})$ breaks down for atoms with a velocity in excess of $[\pi/3s(T)]^{1/2}\bar{v}$, as this leads to a sticking probability of more than unity. Therefore, for large $[s(T) > 0.25]$ sticking coefficients we expect this model to be insufficiently accurate. The model is also suspect in the low-temperature limit, as theory predicts $s(\mathbf{v}) \sim v$. In fact, recent experiments have shown that for helium films $s(\mathbf{v})$ need not even be monotonous in T at low temperature,[33] possibly due to substrate effects.[45,46] Furthermore, the $\cos\theta$ angular dependence of $s(\mathbf{v})$ as suggested by sim-

FIG. 12. The transmission coefficient K as function of the length over radius quotient L/a for several fixed atomic sticking probabilities.

ple theory is only approximately correct outside the low-temperature $[s(\mathbf{v}) \sim \sqrt{T}]$ regime. The result of the new simulation therefore only indicates the influence of the particular model used to analyze our data.

The simulation starts with an atom placed at a random location in the entrance of the capillary having a speed generated with the relation $u_y = (y + 1)\exp(-y)$ with $y = (mv^2)/(2k_BT)$ and u_y a uniformly distributed random number in the range $0 < u_y < 1$. The direction of departure is chosen randomly according to a cosine distribution. When a wall collision occurs, the atom has the probability $s(\mathbf{v}) = \frac{3}{4}s(T)y\cos\theta$ to stick to the surface. After sticking, the speed of the atom is determined by $u_y = (\frac{1}{2}y^2 + y + 1)\exp(-y)$ to comply with the detailed balance. The result may be described to within 0.7% relative error in $s(K)$ in the range $0.03 < s < 0.25$ by the empirical formula

$$s(K) = 0.134e^{3.2(1-K)^4} + 1.17e^{0.075(1-K)}$$
$$-0.09(0.5 - K)^3 - 1.31525 . \qquad (53)$$

This formula may be extended to the interval $0 \leq s \leq 0.35$ while the relative error between this formula and the results of the simulation remains $< 1.5\%$. This result is also shown in Fig. 13.

The models on which the computer simulations are based clearly represent a simplified picture of the physics involved. The measurements are sensitive for any process that leads to momentum transfer in the direction along the axis of the capillary tube. This is most effectively done by atoms that stick some time to the surface, but more generally results from any inelastic scattering process or surface roughness. Hence our models tend to overestimate s. This is in particular the case for the velocity-dependent model in which the contribution to the transmission by atoms at grazing incidence is disproportionally large. In view of the theoretical assertion[23,39,47] that the sticking channel is most effective in exchanging energy and momentum between gas and surface it seems reasonable to assume that the effect of inelastic scattering is small compared to the experimental accuracy.

The results of the experiment based on the one-speed model and those based on the velocity-dependent model are given in Fig. 14. For ^{4}He the results are shown by the open circles, obtained from pressure decay measurements, and the solid circles, obtained from flux decay measurements. Note the excellent agreement between both methods. Each data point represents the average of at least four measurements, the error bar being the standard deviation of the results, augmented by a small systematic error. The sticking coefficient, based on the velocity-dependent model, substantially differs from our previous analysis. It is still linear in temperature, but whereas the previous analysis resulted in a sticking coefficient which may be described as $s/T = 0.33(3)$ K^{-1} for 145 mK$< T < 526$ mK, the new analysis renders $s/T = 0.65(6)$ K^{-1} in the same temperature range.

Due to the inherent shortcomings of both models to relate s to K it is hard to express a strong preference to one or the other. The uncertainty in the relation between K and s shows this type of experiment to be not very suitable to determine $s(T)$ with precision, although the linear temperature dependence of s appears to be well established. The enhancement in transmission of the velocity-dependent model with respect to the one-speed model is mainly due to the population of low-velocity particles and atoms striking the walls at grazing incidence. As discussed above, it is this population for which the velocity-dependent model is most unreliable. We therefore have a slight preference for the results of the one-speed model although this preference is somewhat speculative.

Adding a small amount of ^{3}He (0.2%) to the ^{4}He in our cell we noticed a clear reduction of the recombination rate, indicating a reduction of the binding energy and implying a definite change in adsorption potential and in ripplon dispersion (the surface tension falls from $\gamma = 3.54 \times 10^{-4}$ J m^{-2} to $\gamma = 1.53 \times 10^{-4}$ J m^{-2} when changing from pure ^{4}He to pure ^{3}He surfaces).[43,44,63] However within experimental error no effect was observed on s (open triangles in Fig. 14). Increasing the ^{3}He fraction to 5% a small (about 10%) increase in s was observed at 164 mK with the pressure gauge (open square). Under these conditions we estimate the local ^{3}He concentration in the cell to be at least 30% and hence expect H↓ to scat-
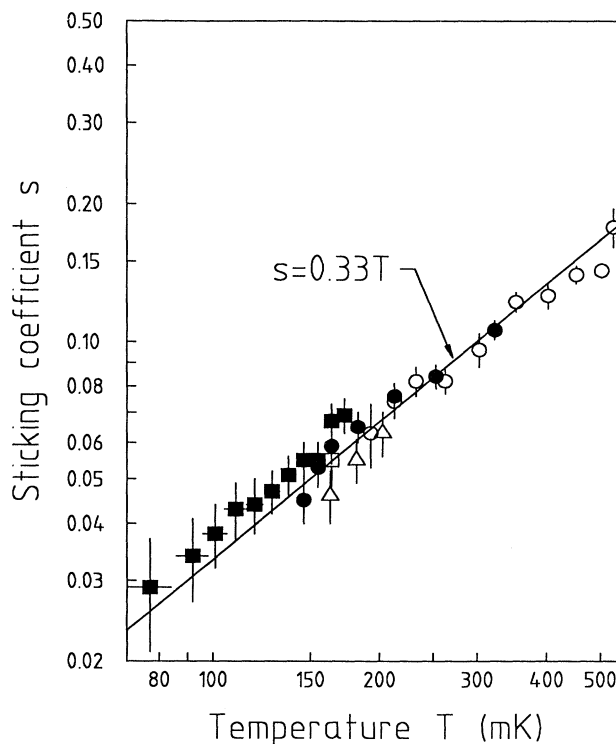

FIG. 14. The sticking coefficient as a function of temperature, based on a model with fixed atomic sticking coefficient. Solid line: $s = 0.33T$. Open circles: pure ^{4}He surface, pressure decay measurements; solid circles: pure ^{4}He surface, flux decay measurements; open triangles: mixture with 0.2% ^{3}He, pressure decay measurements; open square: mixture with 5% ^{3}He, pressure decay measurement; solid squares: mixture with 5% ^{3}He, flux decay measurements.

ter from a ^{3}He-rich phase. Most of our 5% ^{3}He results, shown as solid squares in Fig. 14, were obtained with the pump plate and are in fair agreement (10%) with the 164 mK pressure gauge result. Adding 50% ^{3}He with the flux decay measurements no change was observed on s. No further pressure measurements could be done as bulk liquid started to collect in the pressure gauge. The results on ^{3}He/^{4}He mixtures in the cell are described by the same formula as those on pure ^{4}He substrates within the range of $73 < T < 174$ mK for our measurements. Although the reliability of our thermometry rapidly decreases below 100 mK the trend of decreasing sticking probabilities with decreasing temperatures clearly continues down to our lowest temperature.

To incorporate the effect of binary gas collisions in our one-speed model, we randomly generated collisions using a mean free path λ corresponding to the local density n in the capillary according to $\lambda = (16\sqrt{2}n\sigma/9\pi)^{-1}$, where σ is a hard-sphere scattering cross section.[64] The local density was based on the wall-collision rate calculated with the same simulation, but neglecting gas collisions. After a gas collision, the test atom was restarted in a random direction, sampling an angular distribution chosen to be isotropic in the laboratory system. We may describe our simulation results for the density dependence of K by

$$K \approx K_0(1 - \sigma\lambda_0 K_0 n) . \tag{54}$$

Here K_0 is the transmission coefficient in the zero density limit and $\lambda_0 \equiv 6.1$ mm is a reference length provided by the simulation. Equation (54) only holds in the extremely rarefied limit. At higher densities K should show the Knudsen minimum before entering the viscous regime.[65] In our measurements $\lambda > 2$ cm, comparable to the length of the capillary. We thus find $c_1 \equiv K_0/\tau_0$ and $c_2 \equiv -\sigma\lambda_0 K_0^2/\tau_0 + K_{\rm rec}$, where $K_{\rm rec}$ is a rate constant accounting for recombination. These expressions show that gas collisions do not affect c_1. To look for effects of gas-phase collisions, we analyzed our pressure decays with pure ^{4}He surfaces to extract c_2. Values for c_2 were obtained starting the fits at a fixed initial density $n_0 = 5 \times 10^{14}$ cm^{-3}. We found $c_2 = -A + B(T - T_{\rm ref})$, with $A = 6.2(15) \times 10^{-17}$ cm^3 s^{-1}, $B = 8(14) \times 10^{-17}$ cm^3 s^{-1} K^{-1}, and $T_{\rm ref} = 270$ mK. We established experimentally that the contribution of $K_{\rm rec}$ to c_2 was negligibly small. Once σ is extracted from c_2 the coefficient of self-diffusion follows with $D = \frac{1}{3}\bar{v}\lambda$,[64] which is found to be temperature independent within experimental error. Averaging over all data we find $nD = 1.3(5) \times 10^{18}$ cm^{-1} s^{-1}, in good agreement with the theoretical value of Lhuillier $nD = 1.5 \times 10^{18}$ cm^{-1} s^{-1}.[66]

This agreement with theory is rather fortuitous. If we take into account some effect of the speed of the particle from which the atom collides by assigning the atom after collision a velocity according to a random distribution in the reference frame moving with the mean drift speed of the atoms in the capillary at the location of the collision, the results for the diffusion constant change by a factor of 10. Clearly the one-speed test particle method is not suited to accurately account for gas-collisional effects, although the origin of the c_2 term is well established. In

view of the large experimental error in c_2 and the availability of high-quality NMR data for spin diffusion[67] we did not pursue the refinement of simulation methods for gas collisions any further.

B. Mirror reflection experiment

The aim of the MR experiment was to study the H-surface scattering at normal incidence with high angular resolution. The atoms escaping through the orifice in the bottom of the buffer volume give rise to a highly divergent atomic beam in the pumping volume. We observe the influence of the position of the mirror on the density decay time of the H gas in the buffer reservoir. If the center of the mirror coincides with the center of the orifice the atoms in the beam will be specularly reflected back into the reservoir. The net flux through the diaphragm may be expressed as

$$\Phi = \frac{1}{4}n\bar{v}A\chi , \tag{55}$$

with A the area of the orifice and χ a loss factor representing the probability that the atoms are *not* scattered back into the buffer volume. This equation closely resembles Eq. (39), but with χ replacing K. For our setup 100% reflectivity of a perfectly aligned mirror would correspond to $\chi = 0.042$, as limited by geometrical factors and image aberrations such as coma. For densities up to $n = 10^{14}$ cm^{-3} interatomic collisions in the beam are completely negligible. This analysis implies that the leakage from the reservoir may be largely suppressed with the mirror. The total loss factor χ is due to several loss mechanisms, like surface roughness, coma, sticking, etc. For N independent loss mechanisms with loss factors χ_i the total loss factor χ may be written as

$$\chi = 1 - \prod_{i=1}^{N}(1 - \chi_i) . \tag{56}$$

As in the CF experiment, we assume the density decay is given by Eq. (41). The density at a time t is then given by

$$n(t) = \frac{c_1 n_0 e^{-c_1 t}}{c_1 + c_2 n_0 (e^{-c_1 t} - 1)} . \tag{57}$$

We assume the reduction of the density is only due to the escape of atoms from the buffer volume to the pump volume, so the flux is given by

$$\Phi(t) = -dN(t)/dt = -V_e dn(t)/dt . \tag{58}$$

As we no longer could neglect the influence of c_2, we use this exact equation, resulting in

$$\Phi(t) = \frac{c_1 V_e n_0 e^{-c_1 t}}{c_1 + c_2 n_0 (e^{-c_1 t} - 1)} \times \left[c_1 + \frac{c_1 c_2 n_0 e^{-c_1 t}}{c_1 + c_2 n_0 (e^{-c_1 t} - 1)} \right] . \tag{59}$$

We fit this formula to our data to obtain c_1 and c_2. The second-order constant now represents the possible influ-

ence of gas collisions, recombination, and a first-order correction for the time constant (about 0.5 s) of the pump plate flux detector.

A typical measurement is shown in Fig. 15. We plot the observed loss factor

$$\chi \equiv \tau_0/\tau_1 \equiv c_1 \tau_0 \qquad (60)$$

as a function of the vertical position z of the mirror. Here τ_0 is the first-order decay time in the absence of the mirror, defined in Eq. (46), and ranging from 5.1 s at 80 mK to 2.4 s at 400 mK. The results clearly demonstrate the occurrence of specular reflection of the atoms. With the mirror far from focusing conditions, the decay time is only slightly larger than that expected in the absence of a mirror. As the mirror is moved to bring the diaphragm into focus, the decay time starts to increase dramatically. As seen from the figure, the overall resolution of our apparatus is better than 300 μm (FWHM). From each position scan we may extract the minimal χ value ($\chi_{\min}$) for a given temperature and film thickness. The shape of the χ curve is not exactly symmetrical with respect to the position of $\chi_{\min}$. We were able to devise a model which reproduced the observed line shape. This model incorporates the effects of multiple scattering of the H atoms in the mirror compartment and the geometry of this compartment and the mirror itself. We refrained from using this model to fit our data. While the many assumptions on which this model was based were all plausible, as a whole it is rather speculative. Its value lies in the demonstration that the observed line shapes are in principle understood. To obtain consistent results and reduce the influence of noise in the data we fitted each position scan to an empirical function in which the width of the observed curve Ω and the position of $\chi_{\min}$ were treated as free parameters, while for the loss factor far from focus we took the calculated χ_s. The function was chosen to result in a good fit to all measured scans and was of the form

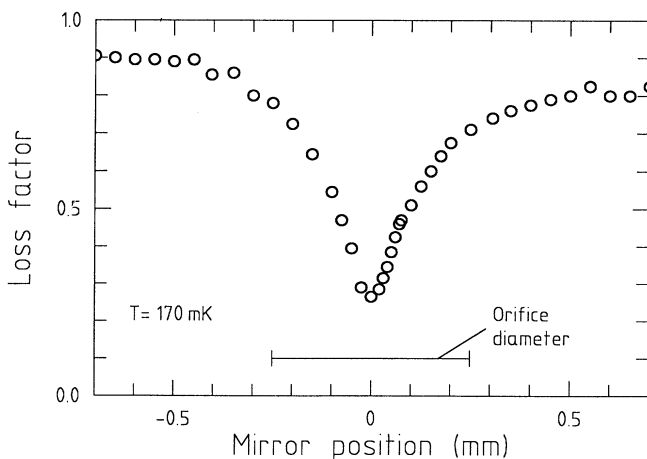$$\chi_s^{-1} + \frac{\chi_{\min}^{-1} - \chi_s^{-1}}{\{1 + [2\sqrt{3}(z - z_0)/\Omega]\}^{1/2}} . \qquad (61)$$

We also analyzed our data with the same function, but treating τ_0 as an additional free parameter. The average of τ_0 over all data agrees within 1% with the calculated value as given by Eq. (45), while individual fits deviated on average about 7%. A summary of our results for $\chi_{\min}$ as a function of temperature is shown in Fig. 16. The triangles represent our data for a saturated ^{4}He film of estimated thickness 115 Å.[68] We purified our ^{4}He with a superleak. The ^{3}He content is ≈ 0.2 ppm. As our measurements of s clearly show the linear dependence on T, the sticking at normal incidence according to theory is given by $s_\perp = \frac{3}{2}s(T) = \gamma_1 T$. The analysis of the CF experiment based on the one-speed model therefore leads to $\gamma_1 = 0.50(5)$ K^{-1}, whereas the analysis based on the velocity-dependent model leads to $\gamma_1 = 1.0(1)$ K^{-1}. The specular reflectivity at normal incidence $R_\perp$ may be estimated using the ansatz $R_\perp = 1 - s_\perp$. For $\gamma_1 = 0.50(5)$ K^{-1} we thus calculate $R_\perp \approx 0.95$ at $T = 100$ mK. For ideal alignment of
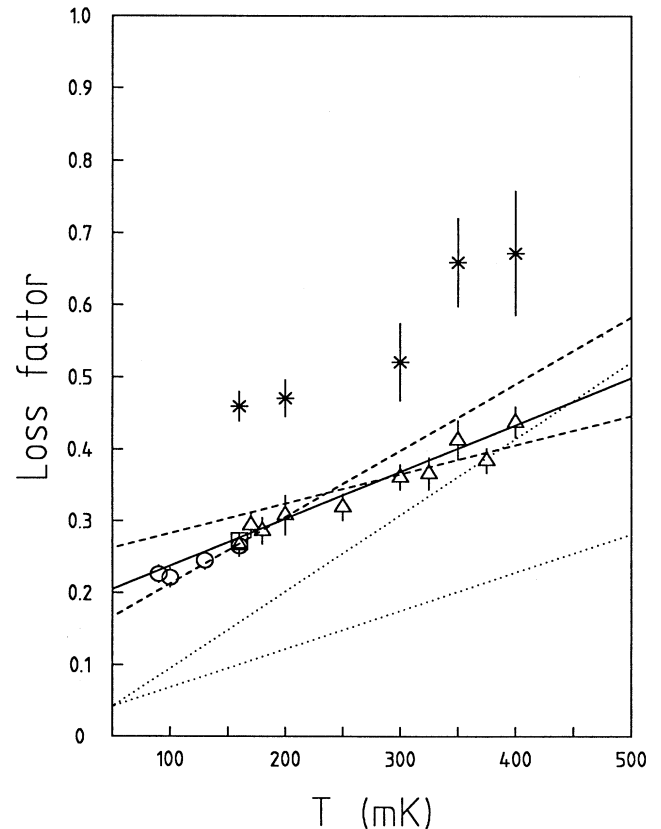

FIG. 16. Measured loss factors as a function of temperature. Crosses: results on thin pure ^{4}He films; triangles: results on saturated ^{4}He films; square: saturated ^{4}He film with partial ^{3}He monolayer coverage; circles: results on saturated ^{4}He films with full ^{3}He monolayer coverage. Dotted lines: expected loss factors with perfect mirror alignment and $s(T) = 0.33T$ ($0.65T$); dashed lines: fits to loss factors under assumption $s(T) = 0.33T$ ($0.65T$); solid line: fit to loss factors, resulting in $s(T) = 0.5T$.

FIG. 15. A typical loss factor measurement.

the optics ($\chi_g = 0.042$) and taking the loss factor due to sticking $\chi_s = s_\perp = \gamma_1 T$, the temperature dependence of $\chi_{\min}$ predicted is indicated by the dotted lines, the lower one assuming $\gamma_1 = 0.50(5)$ K^{-1} and the upper one assuming $\gamma_1 = 1.0(1)$ K^{-1}. Most of the discrepancy with the data may be explained by assuming a lateral misalignment of the mirror or by residual roughness due to surface imperfections of the quartz substrate. Both effects cause a temperature independent loss χ_L from the specular beam,[69] implying that only a lower bound for $R_\perp$ may be extracted from the raw data. For instance, a lateral misalignment of 30 μm of an otherwise perfect mirror leads to $\chi_L = 15\%$. The large loss factors obtained for thin undersaturated films (crosses) may well be understood in terms of substrate roughness.

Assuming $s_\perp = \gamma_1 T$ and fixing $\gamma_1 = 0.5$ K^{-1}, a least squares fit to the saturated helium film data results in $\chi_L = 23\%$ (dashed lines), while fixing $\gamma_1 = 1.0$ K^{-1} results in $\chi_L = 13\%$. These fits poorly describe the data. Alternatively, assuming a linear temperature dependence, $s_\perp = \gamma_1 T$ and treating γ_1 and χ_L as free parameters, fitting Eq. (56) to the data yields the full line characterized by $\chi_L = 17\%$ and $\gamma_1 = 0.74(5)$ K^{-1}. This fit satisfactorily describes our data. The value of γ_1 lies between the values resulting from our determination of s from both models.

In view of the high angular resolution of our experimental setup of 10 mrad even ripplons with wavelength as long as $\lambda = 3000$ Å carry sufficient momentum to deflect H atoms out of the specular beam as defined by the diaphragm. At wavelengths $\lambda \geq 500$ Å the dynamic surface roughness is dominated by thermal ripplons rather than by zero-point fluctuations which are responsible for the sticking process. If we assume that apart from the sticking-desorption process direct (nonsticking) inelastic scattering by ripplons is also of importance, an additional loss factor is present which we shall denote by χ_{in}. The direct inelastic scattering processes neither show up in measurements of α, since they are quasielastic, nor in measurements of s by the capillary flow method, as to first order the momentum along the capillary axis is conserved. The calculation by Hijmans and Shlyapnikov, based on the application of the perturbative scattering theory to direct inelastic scattering, results in $\chi_{\text{in}}(T) = \gamma_2 T^2$ with $\gamma_2 \approx 0.7$ K^{-2} for the probability at normal incidence to scatter out of the specular beam.[26] This result is independent of the exact shape of the H-He potential.[26,27] A least squares fit to the data, assuming $\chi_s = \gamma_1 T$ with fixed $\gamma_1 = 0.5$ K^{-1} (based on our one-speed model and supported by the measurements of the accommodation coefficient of Helffrich et al.[32]) and $\chi_{\text{in}} = \gamma_2 T^2$, yields $\gamma_2 = 0.5(1)$ K^{-2} and $\chi_L = 0.20$ (solid curve). This curve also satisfactorily describes our data. Given both fits discussed we are reluctant to use our data to prove or disprove the existence of another inelastic scattering channel, as reported earlier in our letter.

Evidence for the absence of static surface roughness was obtained by increasing the film thickness by a factor 2, which had no effect on the observed loss factor. We therefore assume χ_L is due to a lateral misalignment of the mirror of about 40 μm. Remarkably, as in the cap-

illary flow experiment, no effect on the reflectivity was observed by adding up to 0.1% ^{3}He to the helium in the cell. Under these conditions the presence of a full monolayer of ^{3}He is to be expected on the surface of the mirror.

VI. CONCLUSIONS

In the capillary flow experiments we observe a strong enhancement of more than a factor 10 of the flow rate in comparison to ordinary Knudsen flow. This is related to a small sticking probability s for the temperature regime studied. For ^{4}He surfaces, using a fixed atomic sticking probability in our model, we find $s/T = 0.33(3)$ K for $145 < T < 526$ mK, while for a velocity-dependent atomic sticking probability we find $s/T = 0.65(6)$ K. We have a slight preference for the first model. In Fig. 17 the results of the one-speed model are compared with all other measurements in this temperature range. In particular the agreement with the results of Helffrich et al. are striking. The experimental results of Doyle et al. are not included in this figure as they apply to a temperature regime starting 1 order of magnitude lower than our lowest results. Their results show an increasing sticking probability with decreasing temperature. Both sets of data need not be conflicting as a local minimum in $s(T)$ may result from substrate induced resonant enhancement of the sticking process as discussed by Goldman, Hijmans and Shlyapnikov, and Carraro and Cole. Within experimental error the transmission through the capillary did not change by adding up to 50% ^{3}He at 150 mK. Results for ^{3}He/^{4}He surfaces were obtained for $73 < T < 174$ mK and are described by the same relations. Our results show that differences between sticking and accommodation coefficients observed in the early experiments are mainly due to differences in temperature of observation.
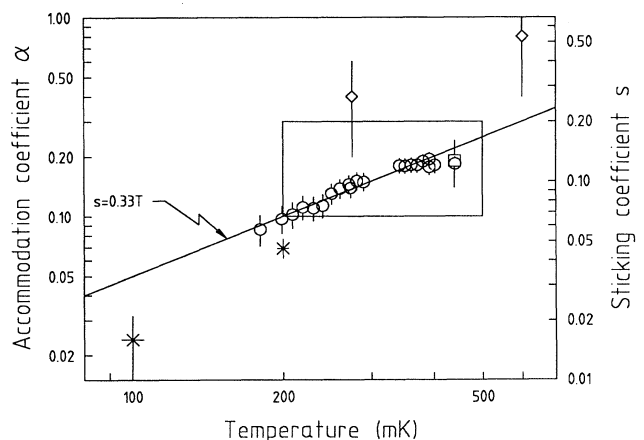

FIG. 17. Sticking probabilities and accommodation coefficients by various authors. Crosses: results of Jochemsen et al. (Ref. 28); big square: result of Salonen et al. (Ref. 30); little square: result of SJKTT (Ref. 31); diamonds: results of Bell et al. (Ref. 9); circles: results of Helffrich et al. (Ref. 32). The results of the CF experiment based on the one-speed model is represented by the straight line $s(T) = 0.33T$.

Surface roughness may also lead to nonspecular reflection. In view of the remarkable smoothness of the inside of the capillary as shown by the scanning electron microscope, combined with the smoothing effect of the helium film, we do not believe surface roughness of the Pyrex substrate influences our data.

In the mirror experiments we measure at normal incidence a lower limit of 80% for the specular reflectivity. Mirror and diaphragm enable us to study the specularly reflected beam with an angular resolution of about 10 mrad. This resolution is sufficiently high to discriminate between specular and near-elastic scattering. However, the method is extremely sensitive for radial misalignment. The coefficient for the direct inelastic process may only be extracted with confidence, if precision data for the sticking coefficient is available.

[1] J.J. Berkhout and J.T.M. Walraven, in *Spin-Polarized Quantum Systems*, edited by S. Stringari (World Scientific, Singapore, 1989), p. 201.

[2] J.T.M. Walraven and J.J. Berkhout, in *Frequency Standards and Metrology*, edited by A. de Marchi (Springer-Verlag, Berlin, 1989), p. 102.

[3] J.T.M. Walraven, in *The Physics of Electronic and Atomic Collisions*, AIP Conf. Proc. No. 205, edited by A. Dalgarno *et al.* (AIP, New York, 1990), p. 599.

[4] J.T.M. Walraven, in *Excitations in Two-Dimensional and Three-Dimensional Quantum Fluids*, edited by A.F.G. Wyatt and H. Lauter (Plenum, New York, 1991), p. 511.

[5] I.F. Silvera and J.T.M. Walraven, in *Progress in Low Temperature Physics*, edited by D.F. Brewer (Elsevier Science, Amsterdam, 1986), Vol. X, p. 139.

[6] R. Sprik, J.T.M. Walraven, and I.F. Silvera, Phys. Rev. Lett. **51**, 479 (1983); **51**, 942 (1983).

[7] H.F. Hess, D.A. Bell, G.P. Kochanski, R.W. Cline, D. Kleppner, and T.J. Greytak, Phys. Rev. Lett. **51**, 483 (1983).

[8] R. Sprik, J.T.M. Walraven, and I.F. Silvera, Phys. Rev. B **32**, 5668 (1985).

[9] D.A. Bell, H.F. Hess, G.P. Kochanski, S. Buchman, L. Pollack, Y.M. Xiao, D. Kleppner, and T.J. Greytak, Phys. Rev. B **34**, 7670 (1986).

[10] T.J. Tommila, S. Jaakkola, M. Krusius, I. Krylov, and E. Tjukanov, Phys. Rev. Lett. **56**, 941 (1986).

[11] T.J. Tommila, E. Tjukanov, M. Krusius, and S. Jaakkola, Phys. Rev. B **36**, 6837 (1987).

[12] J.D. Gillaspy, I.F. Silvera, and J.S. Brooks, Phys. Rev. B **38**, 9231 (1988).

[13] H.F. Hess, G.P. Kochanski, J.M. Doyle, N. Masuhara, D. Kleppner, and T.J. Greytak, Phys. Rev. Lett. **59**, 672 (1987).

[14] R. van Roijen, J.J. Berkhout, S. Jaakkola, and J.T.M. Walraven, Phys. Rev. Lett. **61**, 931 (1988).

[15] N. Masuhara, J.M. Doyle, J.C. Sandberg, D. Kleppner, T.J. Greytak, H.F. Hess, and G.P. Kochanski, Phys. Rev. Lett. **61**, 935 (1988).

[16] J.M. Doyle, J.C. Sandberg, N. Masuhara, I.A. Yu, D. Kleppner, and T.J. Greytak, J. Opt. Soc. Am. B **6**, 2244 (1989).

[17] T.W. Hijmans, O.J. Luiten, I.D. Setija, and J.T.M. Walraven, J. Opt. Soc. Am. B **6**, 2235 (1989).

[18] R.V.E. Lovelace, C. Mehanian, T.J. Tommila, and D.M. Lee, Nature (London) **318**, 30 (1985).

[19] H.F. Hess, Phys. Rev. B **34**, 3476 (1986).

[20] T.J. Tommila, Europhys. Lett. **2**, 789 (1986).

[21] J.J. Berkhout, E.J. Wolters, R. van Roijen, and J.T.M. Walraven, Phys. Rev. Lett. **57**, 2387 (1986).

[22] J.J. Berkhout, O.J. Luiten, I.D. Setija, T.W. Hijmans, T. Mizusaki, and J.T.M. Walraven, Phys. Rev. Lett. **63**, 1689 (1989).

[23] Yu. Kagan, G.V. Shlyapnikov, and N.A. Glukhov, Pis'ma Zh. Eksp. Teor. Fiz. **40**, 287 (1984) [JETP Lett. **40**, 1072 (1984)].

[24] B. Castaing and M. Papoular, J. Phys. Lett. **44**, L537 (1983).

[25] For a compilation of measurements of the binding energy of H on He see W.N. Hardy, M.D. Hürlimann, and R.W. Cline, *Proceedings of the 18th International Conference on Low Temperature Physics, LT-18* [Jpn. J. Appl. Phys. **26**, 2065 (1987)].

[26] T.W. Hijmans and G.V. Shlyapnikov, Phys. Lett. **142**, 45 (1989).

[27] E. Tiesinga, H.T.C. Stoof, and B.J. Verhaar, Phys. Rev. B **41**, 8886 (1990).

[28] R. Jochemsen, M. Morrow, A.J. Berlinsky, and W.N. Hardy, Phys. Rev. Lett. **47**, 852 (1981).

[29] M. Morrow and W.N. Hardy, Can. J. Phys. **61**, 956 (1983).

[30] K. Salonen, I.F. Silvera, J.T.M. Walraven, and G.H. van Yperen, Phys. Rev. B **25**, 6002 (1982).

[31] K. Salonen, S. Jaakkola, M. Karhunen, E. Tjukanov, and T. Tommila, in *Proceedings of the 17th International Conference on Low Temperature Physics, LT-17, Karlsruhe*, edited by U. Eckern, A. Schmid, W. Weber, and H. Wühl (Elsevier Science, Amsterdam, 1984), p. 543.

[32] J. Helffrich, M. Maley, M. Krusius, and J.C. Wheatley, Phys. Rev. B **34**, 6550 (1986).

[33] J.M. Doyle, J.C. Sandberg, I.A. Yu, C.L. Cesar, D. Kleppner, and T.J. Greytak, Phys. Rev. Lett. **67**, 603 (1991).

[34] I.B. Mantz and D.O. Edwards, Phys. Rev. B **20**, 4518 (1979).

[35] W.C. Stwalley, Chem. Phys. Lett. **88**, 404 (1982).

[36] D.S. Zimmerman and A.J. Berlinsky, Can. J. Phys. **61**, 508 (1983).

[37] I.F. Silvera and V.V. Goldman, Phys. Rev. Lett. **45**, 915 (1980).

[38]Yu. Kagan and G.V. Shlyapnikov, Phys. Lett. **95A**, 309 (1983).

[39]B.W. Statt, Phys. Rev. B **32**, 7160 (1985).

[40]D.S. Zimmerman and A.J. Berlinsky, Can. J. Phys. **62**, 590 (1984).

[41]M.W. Cole, Phys. Rev. B **2**, 4239 (1970).

[42]G.D.L. Webster, M. Chester, E. Webster, and T. Oestereich, J. Low Temp. Phys. **40**, 207 (1980).

[43]M. Iino, M. Suzuki, and A.J. Ikushima, J. Low Temp. Phys. **61**, 155 (1985).

[44]D.O. Edwards and W.F. Saam, Prog. Low Temp. Phys. **VIIA**, 283 (1978).

[45]T.W. Hijmans, J.T.M. Walraven, and G.V. Shlyapnikov, Phys. Rev. B **45**, 2561 (1992).

[46]C. Carraro and M.W. Cole, Phys. Rev. B **45**, 12 930 (1992).

[47]V.V. Goldman, Phys. Rev. Lett. **56**, 612 (1986).

[48]Oxford Instruments Limited, Osney Mead, Oxford OX2 0DX, England.

[49]The characteristics of the germanium of this bolometer are given in H.D. Drew and A.J. Sievers, Appl. Opt. **8**, 2067 (1969).

[50]G.H. van Yperen, J.T.M. Walraven, and I.F. Silvera, Phys. Rev. B **30**, 2386 (1984).

[51]R. Sprik, J.T.M. Walraven, G.H. van Yperen, and I.F. Silvera, Phys. Rev. B **34**, 6172 (1986).

[52]J.J. Berkhout, O.H. Höpfner, E.J. Wolters, and J.T.M. Walraven, Proceedings of the 18th International Conference on Low Temperature Physics, LT-18 [Jpn. J. Appl. Phys. **26**, 231 (1987)].

[53]Emerson and Cuming, Inc.

[54]IMI Titanium, P.O. Box 704, Witton, Birmingham B6 7UR, England.

[55]A.F. Harvey, Microwave Engineering (Academic, London, 1963).

[56]Certified grade according to ASTM f68/77, manufactured by Outokumpu Oy, Finland.

[57]P. Clausing, Ph.D. thesis, University of Leiden, Leiden, 1928.

[58]A.S. Berman, J. Appl. Phys. **36**, 3356 (1965).

[59]P. Clausing, Ann. Phys. **12**, 961 (1932).

[60]W.C. De Marcus, in Advances in Applied Mechanics, edited by L. Tabbot (Academic, New York, 1961), Suppl. 1, p. 161.

[61]G.A. Bird, Molecular Gas Dynamics (Clarendon, Oxford, 1976).

[62]K. Yamamoto, J. Hara, and K. Hirose, J. Phys. Soc. Jpn. **51**, 3729 (1982).

[63]A.P.M. Matthey, J.T.M. Walraven, and I.F. Silvera, Phys. Rev. Lett. **46**, 668 (1981).

[64]J.O. Hirschfelder, C.F. Curtiss, and R.B. Bird, Molecular Theory of Gases and Liquids (Wiley, New York, 1954).

[65]M. Knudsen, Ann. Phys. (Leipzig) **28**, 75 (1908).

[66]C. Lhuillier, J. Phys. (Paris) **44**, 1 (1983).

[67]D.M. Lee, Proceedings of the 18th International Conference on Low Temperature Physics, LT-18 [Jpn. J. Appl. Phys. **26**, 1841 (1987)].

[68]To estimate the film thickness we use the formula $m_{He}gh = V(d)$ with $V(d) = \alpha(d)d^{-3}$. For $d = 0$ we use $\alpha = 1.61 \times 10^{-50}$ kg m^5 s^{-2} (Ref. 42), while we assume $\alpha(115 \text{ Å}) \approx 0.75\alpha(0)$ [D.F. Brewer, in The Physics of Liquid and Solid Helium, edited by K.H. Bennerman and J.B. Ketterson (Wiley, New York, 1978), Part II, p. 584].

[69]As pointed out to us by Dr. M. Papoular, static roughness with a needlelike shape and a diameter comparable to the thermal wavelength of the atoms may also result in a temperature dependence. The presence of this type of surface roughness is unlikely in view of the employed polishing procedure.